CHAPTER 3

Linear quantum measurement of mechanical motion

CONTENTS

In this chapter we use the quantum theory of continuous measurement to describe the linearised interaction between light and a mechanical oscillator in a cavity optomechanical system, and quantify how the optical output field can be used to monitor the quantum state of the mechanics. We show that continuous measurement results in unavoidable quantum back-action that heats the mechanical oscillator and introduces a standard quantum limit to force and displacement sensing, and detail how important parameters in quantum optomechanics, including optomechanical coupling rate, cooperativity, and oscillator temperature, can be characterised by optical measurement.

3.1 FREE-MASS STANDARD QUANTUM LIMIT

Before introducing the effects of quantum measurement on the dynamics and precision of cavity optomechanical systems, it is illustrative to consider the simple example of quantum measurement of the position of a free-mass. Specifically, we wish to determine the position of the mass after some time τ by performing two sequential position measurements and are interested in the effect of measurement back-action on the precision [327, 63, 215, 44]. In its continuous limit [46, 65, 64] this is a scenario that is relevant, for example, in interferometric gravitational wave observatories that seek to observe ripples in space-time via the length changes they induce in an interferometer. Current earth-based observatories target gravitational waves with frequencies in the range of a kilohertz and have kilogram-scale suspended end-mirrors with fundamental resonance frequencies in the hertz range. Consequently, on the characteristic time scale of the gravitational waves, the end-mirrors can very well be thought of as free masses.

If the initial measurement localises the position of the mass with a standard deviation $\sigma[\hat{q}(0)]$, the Heisenberg uncertainty principle (Eq. (1.12)) tells us that the measurement must also introduce quantum back-action on the

momentum of the oscillator, increasing its uncertainty to at least

$$\sigma[\hat{p}(0)] = \frac{\hbar}{2\sigma[\hat{q}(0)]}. \tag{3.1}$$

The mass will then freely evolve until the second measurement is performed at time τ. This evolution is, of course, governed by the Hamiltonian

$$\hat{H} = \frac{\hat{p}^2}{2m}, \tag{3.2}$$

which, using the Heisenberg equation of motion (Eq. (1.20)), yields the evolution

$$\hat{q}(\tau) = \hat{q}(0) + \frac{\tau}{m}\hat{p}(0). \tag{3.3}$$

The second measurement can, in principle, be performed with arbitrary precision without any back-action penalty on the position estimate since any back-action effects that it introduces will only alter the dynamics at future times. The uncertainty in the measurement outcome is then entirely specified by $\sigma^2[\hat{q}(\tau)]$, which includes only the uncertainty in the initial localisation of the mass $\sigma[\hat{q}(0)]$ and the component of the mass's momentum uncertainty that has coupled into position during the evolution

$$\begin{aligned}
\sigma^2[\hat{q}(\tau)] &= \sigma^2\left[\hat{q}(0) + \frac{\tau}{m}\hat{p}(0)\right] && (3.4)\\
&= \sigma^2[\hat{q}(0)] + \left(\frac{\tau}{m}\right)^2 \sigma^2[\hat{p}(0)] && (3.5)\\
&= \sigma^2[\hat{q}(0)] + \left(\frac{\hbar\tau}{2m}\right)^2 \frac{1}{\sigma^2[\hat{q}(0)]}. && (3.6)
\end{aligned}$$

Here, by simply taking the sum of the uncertainty contributions from the position and momentum, we are assuming that the position and momentum of the mass are not correlated after the first measurement.[1] Indeed, no such correlations can exist if the mass is in a minimum uncertainty state, as described by Eq. (3.1). The regime in which this assumption breaks down is interesting and can allow improved measurement precision. We consider this regime in some detail in Chapter 5.

Since Eq. (3.6) contains terms that scale both as $\sigma^2[\hat{q}(0)]$ and as $\sigma^{-2}[\hat{q}(0)]$, it is clear that an optimal measurement precision exists that maximises the accuracy of the measurement. It is straightforward to show that this optimum is

$$\sigma_{sql}[\hat{q}(0)] = \sqrt{\frac{\hbar\tau}{2m}}, \tag{3.7}$$

which yields a *standard quantum limit* to position measurement of a free mass

$$\sigma_{sql}[\hat{q}(\tau)] = \sqrt{\frac{\hbar\tau}{m}}. \tag{3.8}$$

[1] Or, specifically, that $\langle\hat{q}(0)\hat{p}(0) + \hat{p}(0)\hat{q}(0)\rangle - 2\langle\hat{p}(0)\rangle\langle\hat{q}(0)\rangle = 0$.

We see therefore that the presence of quantum measurement back-action provides a fundamental limit to the precision of position measurements. To take an example, since gravitational waves cause an oscillation in the relative length of the two arms of an interferometer, a differential position measurement is most sensitive to them if the first measurement is made when one arm of the interferometer is fully extended and the second is made when it is fully contracted. Consequently, detection of a kilohertz gravity wave requires measurements with a delay of around a millisecond. If the end-mirrors have a kilogram mass, Eq. (3.8) gives a standard quantum limited precision of 4×10^{-19} m, within an order of magnitude of the current sensitivity of state-of-the-art ground-based gravitational wave interferometers.

3.2 RADIATION PRESSURE SHOT NOISE

For the majority of the remainder of this chapter we will examine the continuous limit of this measurement back-action and its consequences for the precision of position and force sensors. We begin in this section by considering the effect of fluctuations in radiation pressure due to optical shot noise on the dynamics of a mechanical oscillator. This radiation pressure shot noise is the necessary quantum back-action on the oscillator that compliments the information imprinted on the optical field about the position of the oscillator.

3.2.1 Optomechanical dynamics with on-resonance optical driving

Here we will consider only the linearised dynamics of the optomechanical system (as discussed in Section 2.7), taking the limit where a bright optical field is injected into the cavity and the system is far away from the single photon strong coupling regime (see Chapter 6 for a discussion of this regime). We will, further, take the Markovian limit where the bath has no memory, for both the optical field and the mechanical oscillator, and make the rotating wave approximation on the optical field, taking the cavity resonance frequency to be much higher than any other rates in the problem. In this regime, linearised equations of motion for the dimensionless position and momentum of the mechanical oscillator and optical field can be derived from the Hamiltonian of Eq. (2.41) using the quantum Langevin equations Eqs. (1.90) and (1.112), respectively, for the mechanical oscillator and optical field. The resulting equations of motion are

$$\dot{\hat{X}} = -\frac{\kappa}{2}\hat{X} + \sqrt{\kappa}\hat{X}_{\rm in} \tag{3.9a}$$

$$\dot{\hat{Y}} = -\frac{\kappa}{2}\hat{Y} + \sqrt{\kappa}\hat{Y}_{\rm in} - 2g\hat{Q} \tag{3.9b}$$

$$\dot{\hat{Q}} = \Omega\hat{P} \tag{3.9c}$$

$$\dot{\hat{P}} = -\Omega\hat{Q} - \Gamma\hat{P} + \sqrt{2\Gamma}\hat{P}_{\rm in} - 2g\hat{X}, \tag{3.9d}$$

where we have taken the case of on-resonance optical driving ($\Delta = 0$) for simplicity, and we remind the reader that as usual $\hat{X}$ and $\hat{Y}$ refer to the optical amplitude and phase quadratures, $\hat{Q}$ and $\hat{P}$ refer to the dimensionless mechanical position and momentum, κ and Γ are the optical and mechanical decay rates, and g is the coherent amplitude boosted optomechanical coupling rate. The non-zero detuning case is very interesting and allows cooling, light-mechanical entanglement, and measurements beyond the standard quantum limit. We consider those scenarios in Chapters 4 and 5. Notice that, as might be expected and was discussed in the previous chapter, the position of the mechanical oscillator is imprinted on the phase (or momentum) quadrature of the intracavity field, while the amplitude (or position) quadrature of the optical field is similarly imprinted on the momentum of the mechanical oscillator.

Because we have chosen to drive the optical cavity on resonance ($\Delta = 0$), the quantum stochastic equations describing the optical amplitude and phase quadratures (Eqs. (3.9a) and (3.9b)) are independent. This is not the case for the mechanical oscillator. However, the two first-order stochastic differential equations (Eqs. (3.9c) and (3.9d)) describing the mechanical oscillator are easily combined into a single second-order differential equation

$$\ddot{\hat{Q}} + \Gamma\dot{\hat{Q}} + \Omega^2\hat{Q} = \sqrt{2\Gamma}\Omega\hat{P}_{\rm in} - 2g\Omega\hat{X}. \tag{3.10}$$

This linear system of equations can then be solved straightforwardly in the frequency domain. Taking the Fourier transform, we obtain the steady-state solutions

$$\hat{X}(\omega) = \frac{\sqrt{\kappa}\hat{X}_{\rm in}}{\kappa/2 - i\omega} \tag{3.11a}$$

$$\hat{Y}(\omega) = \frac{\sqrt{\kappa}\hat{Y}_{\rm in} - 2g\hat{Q}}{\kappa/2 - i\omega} \tag{3.11b}$$

$$\hat{Q}(\omega) = \chi(\omega)\left(\sqrt{2\Gamma}\hat{P}_{\rm in} - 2g\hat{X}\right) \tag{3.11c}$$

where the mechanical susceptibility $\chi(\omega) \equiv \Omega/(\Omega^2 - \omega^2 - i\omega\Gamma)$, and we have neglected the ω arguments on the right-hand side and in subsequent analysis. The mechanical susceptibility derived here is identical to that derived in Chapter 1 in the absence of optical driving (Eq. (1.102)), showing that for zero detuning ($\Delta = 0$) the optical field does not modify the response of the mechanical oscillator to its environment. We will see later that this is no longer true if the optical cavity is detuned.

Substituting Eq. (3.11a) for the optical amplitude quadrature into Eq. (3.11c), we arrive at the expression for the mechanical position

$$\hat{Q}(\omega) = \sqrt{2\Gamma}\chi(\omega)\left(\hat{P}_{\rm in} - \sqrt{2C_{\rm eff}}\hat{X}_{\rm in}\right), \tag{3.12}$$

where we have introduced the *effective optomechanical cooperativity*

$$C_{\rm eff}(\omega) \equiv \frac{C}{(1 - 2i\omega/\kappa)^2} \tag{3.13}$$

with C being the *optomechanical cooperativity*

$$C \equiv \frac{4g^2}{\kappa\Gamma}. \tag{3.14}$$

We see that, through radiation pressure, the optical shot noise contributes a heating term to the mechanical oscillator dynamics, with magnitude dependent on the effective optomechanical cooperativity. As might be expected, this heating is attenuated at frequencies above the cavity bandwidth ($\omega > \kappa$) since the incident optical fluctuations at these frequencies are off-resonance and therefore partially rejected from the cavity. Particularly in the resolved sideband regime where $\Omega > \kappa$ that we consider in detail in Chapters 4 and 5, this attenuation has the effect of reducing the optomechanical interaction strength. However, this does not pose a fundamental constraint. Cavity optomechanical systems have been proposed and demonstrated that utilise multiple optical resonances to alter the optical response function and thereby ensure that the optical cavity admits optical fluctuations at both the optical carrier frequency and at sidebands spaced by the mechanical resonance frequency away from the carrier (see, for example, [89, 336, 45]).

3.2.2 Effect of detuning

We have seen above that, in the case of zero optical detuning ($\Delta = 0$), the effect of radiation pressure on the mechanical oscillator is solely to introduce additional heating. The dynamics become more complicated when a non-zero detuning is present. In this case, the optical amplitude and phase quadratures are dynamically linked. Mechanical position information encoded on the intracavity phase quadrature is then transferred to the intracavity amplitude quadrature, and can drive the momentum of the mechanical oscillator. This dynamical back-action on the mechanical oscillator acts to modify its susceptibility, and leads to the possibilities of laser cooling, parametric amplification, and other dynamical effects (see Chapter 4).

Exercise 3.1 *Derive equations of motion for the optical field and mechanical oscillator similar to Eqs. (3.9), but including an optical detuning Δ. Solving these equations in the same manner as above, show that the radiation pressure interaction modifies the mechanical susceptibility to*

$$\chi^{-1}(\omega, \Delta) = \chi^{-1}(\omega) - \frac{4g^2\Delta}{(\kappa/2 - i\omega)^2 + \Delta^2}, \tag{3.15}$$

where $\chi(\omega)$ is the bare susceptibility in the absence of the optical field (Eq. (1.102)).

Unlike the bare mechanical susceptibility, in general, the dynamical back-action modified mechanical susceptibility of Eq. (3.15) is not a generalised Lorentzian function. However, in the low frequency limit where $\omega^2 \ll (\kappa/2)^2 +$

Δ^2 it can be shown to have approximately the same functional form as Eq. (3.15), with modified decay rate $\Gamma(\Delta)$ and frequency $\Omega(\Delta)$ given by

$$\frac{\Gamma(\Delta)}{\Gamma} = 1 + C\,\frac{\Delta\kappa^2\Omega}{\left(\kappa^2/4+\Delta^2\right)^2} \tag{3.16a}$$

$$\frac{\Omega(\Delta)}{\Omega} = \left(1 - \frac{C}{Q}\,\frac{\kappa\Delta}{\kappa^2/4+\Delta^2}\right)^{1/2}, \tag{3.16b}$$

where $Q \equiv \Omega/\Gamma$ is the mechanical quality factor.

Exercise 3.2 *Show these results.*

We can observe from these expressions that, with non-zero detuning, the radiation pressure interaction provides a method to both shift the mechanical resonance frequency, termed the *optical spring effect* and first demonstrated in [259], and, by changing the energy decay rate from the mechanical oscillator without changing its environmental heating rate, to parametrically heat or cool the mechanical oscillator [37, 160]. For further discussion of parametric heating and cooling, and their respective uses to reach the mechanical ground state and generate optomechanical entanglement, the reader is referred to Sections 4.2 and 4.4. From inspection of Eqs. (3.16) it is apparent that the sign of the detuning determines both which of heating or cooling occurs, and whether the optical spring effect pulls the oscillator to higher or lower frequencies. In the special case where the magnitude of detuning $|\Delta| = \kappa/2$, we find that appreciable cooling/heating occurs once the optomechanical cooperativity $C \sim \kappa/\Omega$, while the optical spring effect induces a frequency shift comparable to the mechanical resonance frequency when $C \sim Q$.

3.2.3 Mechanical power spectral density with on-resonance optical driving

Let us now return to the zero-detuning case. Calculating the position power spectral density of the mechanical oscillator using Eq. (1.43), we find

$$S_{QQ}(\omega) = 2\Gamma|\chi(\omega)|^2\left(S_{P_{\rm in}P_{\rm in}}(\omega) + 2\,|C_{\rm eff}(\omega)|\,S_{X_{\rm in}X_{\rm in}}(\omega)\right), \tag{3.17}$$

where we have assumed that the optical and mechanical baths are independent and uncorrelated and therefore neglected the cross terms.

Exercise 3.3 *Assuming that the optical field is of sufficiently high frequency that the optical bath is essentially in a vacuum state, show that within the quantum optics approximation (see Section 1.3.2) the power spectral densities*

$$S_{QQ}(\omega) = 2\Gamma|\chi(\omega)|^2\left(\bar{n} + |C_{\rm eff}(\omega)| + 1\right) \tag{3.18a}$$

$$S_{QQ}(-\omega) = 2\Gamma|\chi(\omega)|^2\left(\bar{n} + |C_{\rm eff}(\omega)|\right). \tag{3.18b}$$

Then, treating the effective optomechanical cooperativity as constant across the mechanical resonance, show that the radiation pressure shot noise raises the mean occupancy $\bar{n}_b$ of the mechanical oscillator in thermal equilibrium from $\bar{n}$ to

$$\bar{n}_b = \bar{n} + \bar{n}_{ba}, \tag{3.19}$$

where

$$\bar{n}_{ba} \equiv |C_{\text{eff}}(\Omega)| = \frac{C}{1 + 4(\Omega/\kappa)^2} \tag{3.20}$$

quantifies the increase in mechanical phonon occupancy due to radiation pressure back-action.

Hint: in the rotating frame the optical bath power spectral density $S_{X_{\text{in}}X_{\text{in}}}(\omega) = \bar{n}_L + 1/2$ (see Section (1.4.6)), with $\bar{n}_L$ being the photon occupancy of the incident optical field evaluated at the laser carrier frequency Ω_L.

Equation (3.19) makes the physical significance of the effective optomechanical cooperativity C_{eff} quite clear. It establishes the optomechanical coupling strength required for the optical back-action on the mechanical oscillator to heat the oscillator by one phonon. As we will see in later chapters, the optomechanical cooperativity has other significance as well. For instance, it is the metric that establishes the effectiveness of both resolved sideband cooling (see Section 4.2.2) and feedback cooling (see Section 5.2).

Radiation pressure effects are widely seen in experiments with cold atomic gases. For instance, the random recoil experienced by atoms upon spontaneous emission of light sets a limit on the temperature of an atomic ensemble in a magneto-optic trap [177]. However, the radiation pressure back-action heating of a single collective mode of motion that we have introduced here was first observed only in 2008 [207], in that case using a collective mechanical mode of a cloud of 9,000 ultracold atoms. Since the optomechanical cooperativity is proportional to the square of the zero-point motion of the mechanical oscillator, as the mass of the mechanical oscillator increases it becomes increasingly difficult to achieve $|C_{\text{eff}}| > \bar{n}$, as required for radiation pressure shot noise to dominate thermal heating. In 2013 radiation pressure shot noise was observed for the first time for a mechanical resonance of a macroscopic mechanical oscillator using a 7 ng silicon nitride membrane [231] (see Fig. 3.1).

3.3 MEASUREMENT OF MECHANICAL MOTION

As we have just seen, the radiation pressure interaction perturbs the motion of a mechanical oscillator, introducing noise. This noise can be understood to be a direct consequence of the Heisenberg uncertainty principle between position and momentum. The interaction encodes position information on the optical field, necessitating an increase in noise on the mechanical momentum. In this section we introduce the linear detection processes of homodyne and

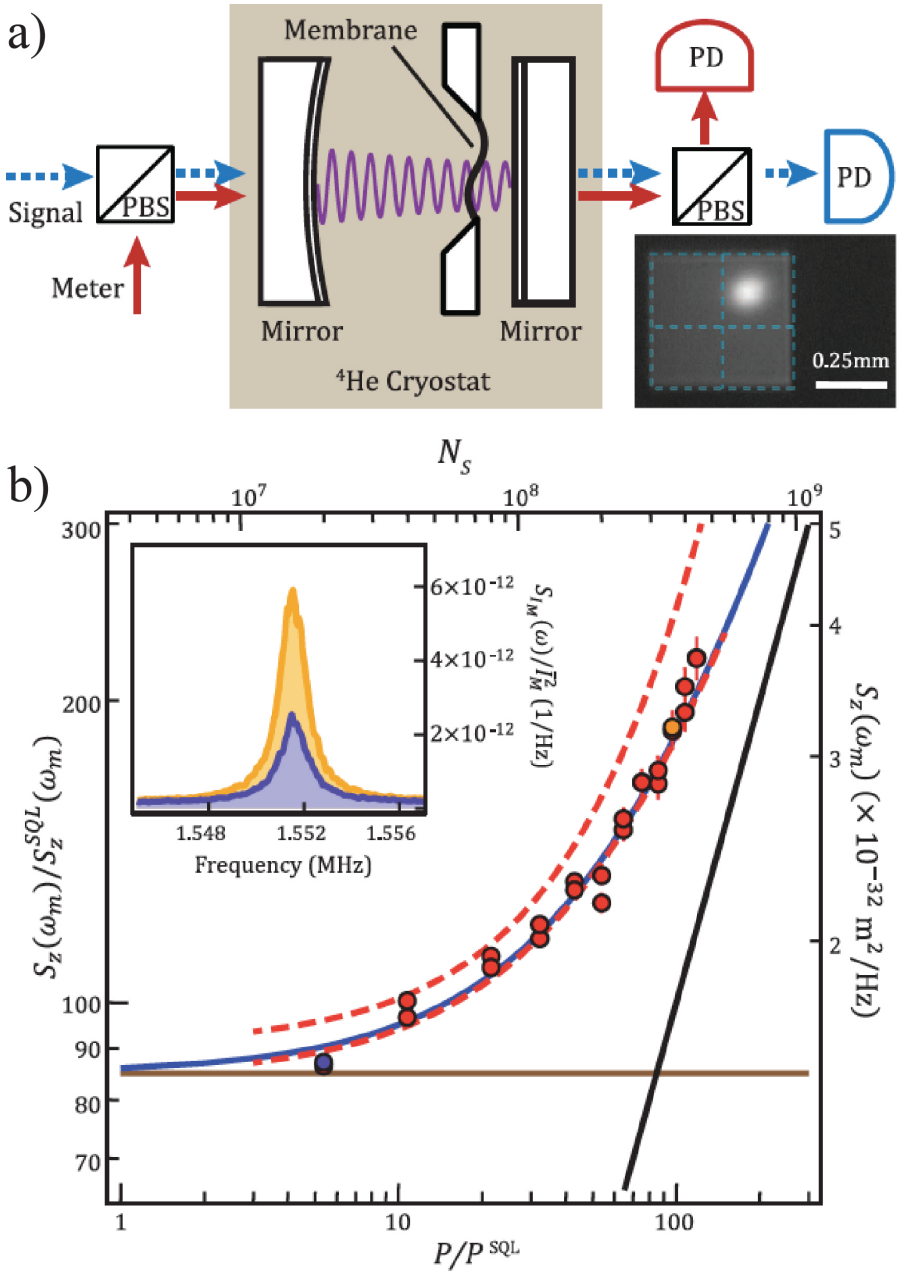

FIGURE 3.1 Observation of measurement back-action on a cryogenically cooled silicon nitride membrane with 7 ng effective mass in a Fabry–Pérot cavity. From [231]. Reprinted with permission from AAAS. (a) Experimental schematic. (b) Peak position power spectral density as a function of incident power showing that the resonant mode temperature increases with power. N_S: intracavity photon number, P/P^{SQL}: ratio of injected power to power at the standard quantum limit, $S_z(\omega_m)$: mechanical power spectral density at the mechanical resonance frequency, $S_z^{\mathrm{SQL}}(\omega_m)$: mechanical power spectral density at the standard quantum limit, $S_{I_M}(\omega)/\bar{I}_M^2$: normalised power spectral density of secondary meter beam, PBS: polarising beam splitter, PD: photodiode.

heterodyne detection commonly used to extract information about the mechanical oscillator from the field that exits the optomechanical system. This will allow us to establish, later in the chapter, standard quantum limits for both mechanical position and force measurement.

Before embarking on this discussion of detection techniques, however, we will establish a formal minimum bound on the product of the measurement imprecision and the magnitude of radiation pressure noise exerted on a mechanical oscillator valid in the case of continuous linear measurements [44].

3.3.1 Quantum bound on force-imprecision product

The force experienced by the mechanical oscillator in an optomechanical system described by the linearised Hamiltonian of Eq. (2.41) may be determined in the usual way via $\hat{F} = \partial\hat{H}/\partial\hat{q}$, where $\hat{q}$ is of course the mechanical position operator. The contribution to this force from the optical field is easily shown to be

$$\hat{F}_L = \frac{\sqrt{2}\hbar g}{x_{zp}}\hat{X}. \tag{3.21}$$

Exercise 3.4 *Convince yourself of this.*

Here the optical amplitude quadrature $\hat{X}$ is driven by the fluctuations of the optical input field $\hat{X}_{\rm in}$, as we already found in Eq. (3.9a). Let us consider, for now, the bad cavity limit where κ is much larger than Ω as well as all other system rates, leaving a more general treatment to later sections. In this simple case $\hat{X}$ reaches equilibrium much faster than any other system variable and Eq. (3.9a) can be adiabatically eliminated via the approximation $\dot{\hat{X}} = 0$. Equation (3.21) can then be expressed in terms of the input optical fluctuations as

$$\hat{F}_L = \sqrt{\frac{8}{\kappa}}\left(\frac{\hbar g}{x_{zp}}\right)\hat{X}_{\rm in}, \tag{3.22}$$

with the radiation pressure force power spectral density given by

$$S_{FF}(\omega) = \frac{8}{\kappa}\left(\frac{\hbar g}{x_{xp}}\right)^2 S_{X_{\rm in}X_{\rm in}}(\omega). \tag{3.23}$$

A similar adiabatic elimination for $\hat{Y}$ in Eq. (3.9b) allows the intracavity optical phase quadrature to be related simply to the mechanical position $\hat{q}$ and input optical phase quadrature fluctuations $\hat{Y}_{\rm in}$ by

$$\hat{Y} = \frac{2}{\kappa}\left(\sqrt{\kappa}\hat{Y}_{\rm in} - \frac{\sqrt{2}g}{x_{zp}}\hat{q}\right). \tag{3.24}$$

The input-output relations given in Eqs. (1.126) then allow the output optical phase quadrature fluctuations to be determined:

$$\hat{Y}_{\rm out} = -\hat{Y}_{\rm in} + \sqrt{\frac{8}{\kappa}}\left(\frac{g}{x_{zp}}\right)\hat{q}. \tag{3.25}$$

The mechanical position could be determined by measuring $\hat{Y}_{\rm out}$, with an ideal measurement only contaminated by the input phase quadrature fluctuations $\hat{Y}_{\rm in}$. By inspection of Eq. (3.25), as long as $\hat{Y}_{\rm in}$ is uncorrelated to the mechanical position, the minimum possible measurement (or imprecision) noise is quantified by the power spectral density

$$S_{qq}^{\rm imp}(\omega) = \frac{\kappa}{8}\left(\frac{x_{zp}}{g}\right)^2 S_{Y_{\rm in}Y_{\rm in}}(\omega). \tag{3.26}$$

We therefore find that the product of imprecision and force noise power spectral densities is

$$S_{FF}(\omega)S_{qq}^{\rm imp}(\omega) = \hbar^2 S_{X_{\rm in}X_{\rm in}}(\omega)S_{Y_{\rm in}Y_{\rm in}}(\omega). \tag{3.27}$$

A Heisenberg uncertainty principle exists between the amplitude and phase quadrature power spectral densities (see Eq. (1.121)). This results in the lower bound on the disturbance from the measurement

$$S_{FF}(\omega)S_{qq}^{\rm imp}(\omega) \geq \left(\frac{\hbar}{2}\right)^2. \tag{3.28}$$

We therefore see that, indeed, linear measurement of mechanical motion will unavoidably result in a quantum back-action force on the mechanical oscillator. While here we arrive at Eq. (3.28) by considering the specific case of continuous measurement on a mechanical oscillator within a bad optical cavity, the expression is quite general, applying to any continuous measurement in the absence of quantum correlations [44]. This leads to standard quantum limits in both position and force measurement. Noncontinuous measurements or measurements that involve nonclassical states of the light or mechanical oscillator can exceed the limit set out in Eq. (3.28). Such schemes form much of the discussion in Chapter 5.

3.3.2 Output field from a cavity optomechanical system

We now return to the primary subject matter of this section, treating the optical field output from a cavity optomechanical system, and approaches to extract information about the mechanical oscillator from this output in a manner that is valid more generally than the bad cavity regime considered in the previous section.

The quadratures of the output optical fields from the cavity optomechanical system can be determined using Eqs. (3.11a) and (3.11b) along with the

input-output relations given in Eqs. (1.126). The result is

$$\hat{X}_{\rm out}(\omega) = -\left(\frac{\kappa/2+i\omega}{\kappa/2-i\omega}\right)\hat{X}_{\rm in} \tag{3.29a}$$

$$\begin{aligned}\hat{Y}_{\rm out}(\omega) &= -\left(\frac{\kappa/2+i\omega}{\kappa/2-i\omega}\right)\hat{Y}_{\rm in} + \frac{2\sqrt{\kappa}g\hat{Q}}{\kappa/2-i\omega} \\ &= -\left(\frac{\kappa/2+i\omega}{\kappa/2-i\omega}\right)\hat{Y}_{\rm in} + 2\sqrt{\Gamma C_{\rm eff}}\hat{Q}.\end{aligned} \tag{3.29b}$$

As expected, we see that both quadratures experience a frequency-dependent phase rotation due to the optical resonance, and the mechanical position is imprinted on the output optical phase quadrature with a magnitude determined by the characteristic rate $\mu = \Gamma|C_{\rm eff}|$.[2] In the nonresolved sideband limit, where $\Omega \ll \kappa$, this rate can be approximated as $\mu = 4g^2/\kappa$. On the other hand, in the resolved-sideband regime as $\Omega/\kappa \to \infty$, the measurement rate $\mu \to 0$ so that the information imprinted on the optical field becomes asymptotically small. This is important for resolved sideband cooling, as discussed in Section 4.2.2, since any information contained in the optical field necessarily introduces a complimentary back-action heating which presents a fundamental limit the cooling performance [191].

3.3.3 Linear detection of optical fields

Although nonlinear techniques such as photon counting [76] or coupling to a superconducting qubit [213] have been implemented to detect the output field of cavity optomechanical systems (see Section 8.2), by far the most common detection techniques are linear, ultimately providing signals that are proportional to the amplitude of the optical field. Such techniques can best be understood through the example of direct detection of a bright field.

When an optical field described in the Heisenberg picture by the annihilation operator $a_{\rm det}(t)$ impinges upon a semiconductor photodiode, photons in the field are converted into photoelectrons, which generates a (nonlinearised) photocurrent that can be described by the detected field operator

$$\hat{i}(t) = \hat{n}_{\rm det}(t) = a^\dagger_{\rm det}(t)a_{\rm det}(t), \tag{3.30}$$

where $\hat{n}_{\rm det}$ is the photon number operator for the detected field and $\langle a_{\rm det}\rangle = \alpha_{\rm det}$ is the coherent amplitude of the field, with $\alpha^*_{\rm det}\alpha_{\rm det}$ being the mean photon flux per second incident on the detector. Linearising the optical field in the usual way by making the substitution $a_{\rm det} \to \alpha_{\rm det} + a_{\rm det}$ and neglecting both the constant term $(\alpha^*_{\rm det}\alpha_{\rm det})$ and the operator product term $(a^\dagger_{\rm det}a_{\rm det})$

[2] While this rate appears to depend linearly on the mechanical decay rate Γ and therefore improve as the quality factor of the mechanical oscillator degrades, this is not the case since Γ also appears in the denominator of the expression for $|C_{\rm eff}|$.

yields the linearised detected field operator

$$\hat{i}(t) = \alpha_{\rm det} a^\dagger_{\rm det} + \alpha^*_{\rm det} a_{\rm det} \quad (3.31)$$
$$= |\alpha_{\rm det}| \hat{X}^{\theta_{\rm det}}_{\rm det}, \quad (3.32)$$

where here $e^{i\theta_{\rm det}} = \alpha_{\rm det}/|\alpha_{\rm det}|$, and the rotated quadrature operator $\hat{X}^\theta_{\rm det}$ is defined in Eq. (1.17a). We can therefore expect that direct detection of an optical field will produce a stochastic photocurrent that is directly proportional to the field quadrature which is oriented in the direction of the coherent amplitude (see Fig. 1.2). As we will see in the next section, however, one must be somewhat careful in this interpretation since $\hat{i}(t)$ is an operator, not a classical variable.

3.3.4 Photocurent power spectral density

Any real classical photocurrent must have a power spectral density that is symmetric in frequency. This is not the case, in general, for $\hat{i}(t)$. In the case of optical detection of mechanical motion considered in this chapter, for example, $\hat{i}(t)$ must necessarily contain a term proportional to $\hat{Q}(t)$, which, as we saw in Section 1.2, is asymmetric in frequency. The resolution to this apparent contradiction is that $\hat{i}(t)$ is still, of course, a quantum operator. It is transformed into a stochastic real classical variable $i(t)$ with a symmetrised power spectral density through the detection process and subsequent irreversible electronic amplification. This observed power spectral density can be calculated formally using Glauber's theory of photo-detection [122]. Using Eq. (1.43) one can immediately calculate the power spectral density $S_{\hat{i}\hat{i}}(\omega)$ of the *operator* $\hat{i}(t)$ through the substitution $\hat{\mathcal{O}}(t) = \hat{i}(t)$. The *photocurrent* $i(t)$, on the other hand, is generated by photon annihilation events at the detector, with the photocurrent power spectral density involving two-time photon coincidences. As recognised by Glauber, to accurately determine the photocurrent the annihilation and creation operators must be normally ordered,[3] so that direct detection of the field $a_{\rm det}$ yields the power spectral density

$$S_{ii}(\omega) = \int_{-\infty}^{\infty} d\tau\, e^{i\omega\tau} \langle a^\dagger_{\rm det}(t+\tau) a^\dagger_{\rm det}(t) a_{\rm det}(t+\tau) \hat{a}_{\rm det}(t) \rangle_{t=0}. \quad (3.33)$$

Using the commutation relation of Eq. (1.114) this can be reexpressed in terms of the symmetrised power spectral density of the photocurrent operator $\bar{S}_{\hat{i}\hat{i}}(\omega)$ as[4]

$$S_{ii}(\omega) = \bar{S}_{\hat{i}\hat{i}}(\omega) - \langle \hat{n}_{\rm det} \rangle \quad (3.34)$$
$$\approx \bar{S}_{\hat{i}\hat{i}}(\omega), \quad (3.35)$$

[3] That is, the creation operators should all appear to the left of the annihilation operators.

[4] Note the ˆ's here to distinguish between a classical variable and the detected field operator.

where Eq. (3.35) is valid within the linearisation approximation, since linearisation of $\bar{S}_{\hat{i}\hat{i}}(\omega)$ results in quadrature variance terms that are amplified by the square of the coherent amplitude of the field. We see, therefore, that photodetection will always produce a symmetrised power spectral density.

Exercise 3.5 *Show this result.*

3.3.5 Phase-referenced detection

In the particular case of a cavity optomechanical system in the steady state with zero detuning ($\Delta = 0$) considered in this chapter, we see from Eqs. (2.43) and (2.44) that the coherent amplitude of the output field $\alpha_{\rm out}$ is real.[5] This means that, if the field is directly detected, $\theta_{\rm det} = m\pi$ where m is an integer, and the measured quadrature is the optical amplitude quadrature. Inspection of Eqs. (3.29) shows that no information about the mechanical oscillator is contained on this quadrature. Hence, direct detection is ineffective for probing the mechanical oscillator when no cavity detuning is present. This necessitates a detuning to be introduced to the optical cavity, or the use of alternative forms of detection that provide a phase reference. *Homodyne* and *heterodyne* detection are two such phase-referenced detection techniques that find broad use in coherent communications, microwave electronics, and quantum optics, as well as quantum optomechanics. These techniques are contrasted to direct detection in Fig. 3.2.

The mathematics of homodyne and heterodyne detection is treated in Appendix A. For the purposes of the majority of this textbook it is only important to know that, by interfering the detected field with a bright local oscillator field of the same carrier frequency, homodyne detection provides a measurement of an arbitrary quadrature $\hat{X}^{\theta}_{\rm det}$ of the detected optical field with normalised power spectral density

$$S^{\rm homo}_{ii}(\omega) = \bar{S}_{X^{\theta}_{\rm det}X^{\theta}_{\rm det}}(\omega). \tag{3.36}$$

Heterodyne detection, on the other hand, uses a carrier frequency offset from the laser frequency Ω_L by $\Delta_{\rm LO}$. Making use of the rotating wave approximation (see Appendix A), this results in the normalised power spectral density

$$\begin{aligned} S^{\rm het}_{ii}(\omega) &= \frac{1}{4}\Big[S_{X_{\rm det}X_{\rm det}}(\Delta_{\rm LO}+\omega) + S_{Y_{\rm det}Y_{\rm det}}(\Delta_{\rm LO}+\omega) \\ &\quad + S_{X_{\rm det}X_{\rm det}}(\Delta_{\rm LO}-\omega) + S_{Y_{\rm det}Y_{\rm det}}(\Delta_{\rm LO}-\omega)\Big]. \end{aligned} \tag{3.37}$$

Here, frequency components at $\Delta_{\rm LO} \pm \omega$ have been "mixed down" to ω by the beating between the detected field and local oscillator.

[5] Remembering that we have defined the intracavity amplitude α to be real.

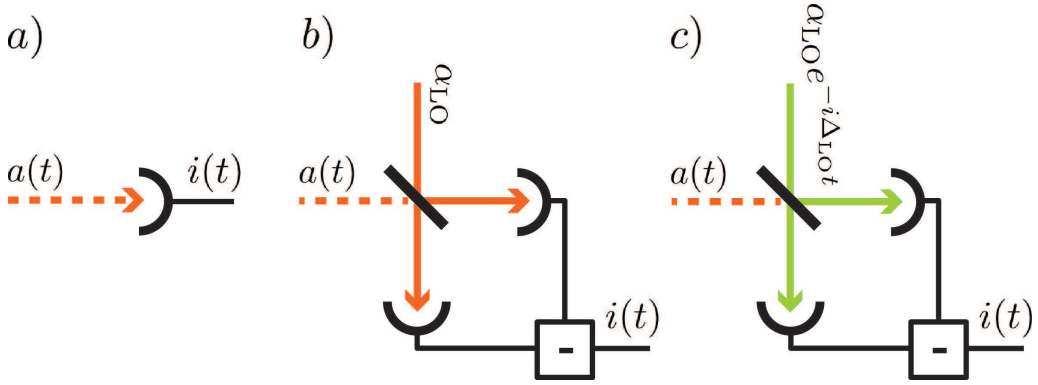

FIGURE 3.2 Schematics of direct (a), homodyne (b), and heterodyne (c) detection of an optical field. $a(t)$ is the input field to be measured. $i(t)$ is the resulting photocurrent. In homodyne detection the input field is interfered on a 50/50 beam splitter with a bright local oscillator that has the same optical carrier frequency. The phase of the local oscillator $\alpha_{\rm LO}$ determines the measured optical quadrature. In heterodyne detection an offset local oscillator carrier frequency is used, resulting in a temporally oscillating phase relative to the input field. The measured optical quadrature therefore also oscillates with time.

3.3.6 Measured power spectral densities from a cavity optomechanical system

Using the result of the previous section, we can determine the power spectral densities of homodyne and heterodyne detection of the optical field output from a cavity optomechanical system. As we have observed previously, Eqs. (3.29) show that, with zero detuning, the amplitude quadrature of the optical field contains no information about the mechanical motion. Consequently, here we consider only the case where $\theta = \pi/2$ so that in the frequency domain the detected quadrature is

$$\hat{X}^{\pi/2}_{\rm det}(\omega) = \hat{Y}_{\rm out}(\omega) \tag{3.38}$$

$$= -\left(\frac{\kappa/2+i\omega}{\kappa/2-i\omega}\right)\hat{Y}_{\rm in}(\omega) - 4\Gamma C_{\rm eff}\chi(\omega)\hat{X}_{\rm in}(\omega) + 2\sqrt{\Gamma C_{\rm eff}}\,\hat{Q}^{(0)}(\omega) \tag{3.39}$$

$$= -\left(\frac{\kappa/2+i\omega}{\kappa/2-i\omega}\right)\hat{Y}_{\rm in}(\omega) + 2\Gamma\sqrt{2C_{\rm eff}}\chi(\omega)\left(\hat{P}_{\rm in}(\omega) - \sqrt{2C_{\rm eff}}\hat{X}_{\rm in}(\omega)\right), \tag{3.40}$$

where

$$\hat{Q}^{(0)}(\omega) \equiv \sqrt{2\Gamma}\chi(\omega)\hat{P}_{\rm in}(\omega) \tag{3.41}$$

is the mechanical position in the absence of measurement (i.e. with $C_{\rm eff} = 0$). Note that, in fact, while the detected signal is maximised for $\theta_{\rm LO} = \pi/2$, correlations between the noise on the output optical amplitude and phase quadratures due the radiation pressure interaction mean that the noise in the measurement – and therefore signal-to-noise ratio – can be reduced by shifting the local oscillator phase away from $\pi/2$. We look into these effects in Chapter 5.

From inspection of Eqs. (3.40) and (3.37) it is clear that the power spectral density of the detected phase quadrature for both homodyne and heterodyne detection contains cross-terms between the mechanical bath fluctuations and the optical input amplitude and phase quadratures. While in principle it is possible for correlations to exist between these baths – for instance, if the mechanical bath consisted of some guided phonon mode that had previously interacted strongly with the optical field – here we treat the usual case where the baths are uncorrelated, so that their cross-spectral densities are zero. This leaves only the cross-spectral densities $S_{X_{\rm in}P_{\rm in}}(\pm\omega)$ and $S_{P_{\rm in}X_{\rm in}}(\pm\omega)$ between the amplitude and phase quadratures of the input field. These are also zero for a coherent or thermal input field, as we found for a general case in Exercise 1.13.

3.3.6.1 Power spectral density from homodyne detection

With no bath correlations, the phase quadrature homodyne power spectral density is simply the sum of the symmetrised power spectral densities of each term in Eq. (3.40):

$$\begin{aligned} S_{ii}^{\rm homo}(\omega) &= \frac{1}{2} + 8\eta\Gamma^2|C_{\rm eff}|^2|\chi(\omega)|^2 + 4\eta\Gamma|C_{\rm eff}|\bar{S}_{Q^{(0)}Q^{(0)}}(\omega) && (3.42)\\ &= \frac{1}{2} + 8\eta\Gamma^2|C_{\rm eff}|\,|\chi(\omega)|^2\left(\bar{n}_b + \frac{1}{2}\right) && (3.43)\\ &= \frac{1}{2} + 4\eta\Gamma|C_{\rm eff}|\bar{S}_{QQ}(\omega), && (3.44)\end{aligned}$$

where $S_{Q^{(0)}Q^{(0)}}(\omega)$ is the power spectral density of the mechanical position in the absence of radiation pressure. To arrive at Eq. (3.43) we have used the nonrotating and rotating frame bath power spectral densities given in Eqs. (1.98) and (1.118a), respectively, for the mechanical bath and optical fields, and have assumed that the optical field has sufficiently high frequency to be well approximated as having no thermal occupancy. To obtain the final expression we have used Eq. (3.18), recognising that the mechanical occupancy includes contributions from both the mechanical bath and the radiation pressure shot noise heating (i.e., $\bar{n}_b = \bar{n} + \bar{n}_{ba}$). The factor of 1/2 at the front of Eqs. (3.43) and (3.44) represents a white background spectrum due to shot noise on the optical field, while the second term is contributed by the mechanical oscillator, including heating from the radiation pressure shot noise driving it.

The perceptive reader will have noticed that the symbol η has been introduced in Eqs. (3.42) to (3.44). This constitutes an overall detection efficiency that accounts for inefficiencies in the escape of the optical field from the cavity, any propagation losses due – for example – to scattering and absorption before the detectors, and inefficiencies in the detection process itself. A discussion of the appropriate approach to model detection efficiencies in the Heisenberg picture is given in Appendix A.

Exercise 3.6 *Derive Eq. (3.43) including detection efficiencies.*

The homodyne power spectral density given in Eq. (3.44) is shown as a function of frequency in Fig. 3.3 for a range of effective cooperativities $C_{\rm eff}$. As can be seen, the thermal noise of the mechanical mode introduces a Lorentzian noise peak to the power spectral density, with the height of the peak increasing as the optomechanical interaction strength increases, due both to improved mechanical transduction and, for $|C_{\rm eff}| > \bar{n}$, radiation pressure shot noise heating.

3.3.6.2 Power spectral density from heterodyne detection

The power spectral density of a heterodyne measurement can be determined in the same way as the homodyne case. Substituting the output optical amplitude and phase quadrature operators from the cavity optomechanical system (Eqs. (3.29)) for $\hat{X}_{\rm det}$ and $\hat{Y}_{\rm det}$ in Eq. (3.37) and using the optical bath power spectral densities defined in Eqs. (1.118a), we find

$$\begin{aligned} S_{ii}^{\rm het}(\omega) &= \frac{1}{2} + \eta\Gamma\Big[\,|C_{\rm eff}(\Delta_{\rm LO}+\omega)|\,S_{QQ}(\Delta_{\rm LO}+\omega) \\ &\quad + |C_{\rm eff}(\Delta_{\rm LO}-\omega)|\,S_{QQ}(\Delta_{\rm LO}-\omega)\Big]. \end{aligned} \tag{3.45}$$

Here, since the power spectrum of the mechanical oscillator $S_{QQ}(\omega)$ is sharply peaked at frequencies $\omega = \pm\Omega$, we can observe that the mechanical peak will appear at four different frequencies offset from $\pm\Delta_{\rm LO}$ by $\pm\Omega$. As long as $\Gamma \ll \Delta_{\rm LO}$ so that the off-mechanical-resonance term in Eq. (3.45) can be neglected, the heterodyne power spectral densities on the positive and negative frequency sides of $\Delta_{\rm LO}$ are

$$S_{ii}^{\rm het}(\Delta_{\rm LO}+\omega) = \frac{1}{2} + \eta\Gamma\,|C_{\rm eff}|\,S_{QQ}(-\omega) \tag{3.46}$$

$$= \frac{1}{2} + 2\eta\Gamma^2\,|C_{\rm eff}|\,|\chi(\omega)|^2\,\bar{n}_b \tag{3.47}$$

$$S_{ii}^{\rm het}(\Delta_{\rm LO}-\omega) = \frac{1}{2} + \eta\Gamma\,|C_{\rm eff}|\,S_{QQ}(\omega) \tag{3.48}$$

$$= \frac{1}{2} + 2\eta\Gamma^2\,|C_{\rm eff}|\,|\chi(\omega)|^2\,(\bar{n}_b+1)\,, \tag{3.49}$$

where we have used Eqs. (3.18) and (3.19), and have again included the overall detection efficiency η, which appears, as in the case of homodyne detection, only as a prefactor attenuating the mechanical signal.

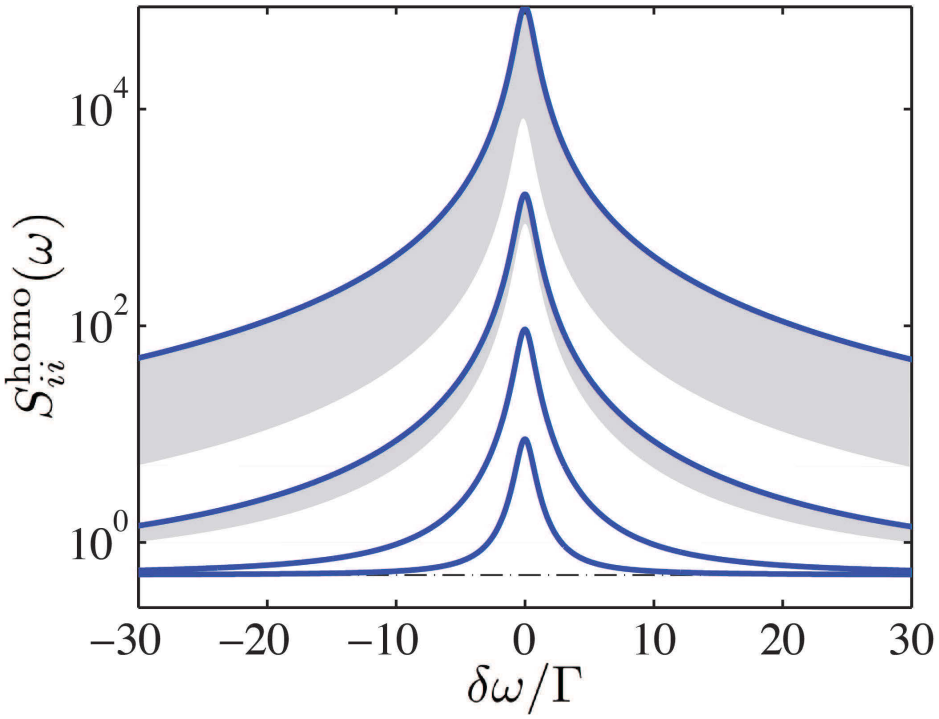

FIGURE 3.3 Photocurrent power spectral density for homodyne phase measurement of the output field from a cavity optomechanical system with cavity detuning $\Delta = 0$ as a function of frequency offset from the mechanical resonance ($\delta\omega = \omega - \Omega$). The effective cooperativities are $|C_{\mathrm{eff}}| = \{0.1, 1, 10, 100\}$, for the bottom to top traces, respectively. The shaded regions, visible only for the top two traces, are the additional noise power introduced by radiation pressure shot noise heating. The dot-dashed line is the optical shot noise level. For each trace the thermal occupancy is $\bar{n} = 10$, the mechanical quality factor is $Q = \Omega/\Gamma = 1000$, and the measurement efficiency is taken to be unity ($\eta = 1$).

The above power spectral densities are similar to that obtained using homodyne detection in Eq. (3.43). However, there are two notable differences. Firstly, the mechanical signal here is attenuated by a factor of four; a factor of two arises from the fact that heterodyne detection is sensitive to both the amplitude and phase quadratures of the detected light field, while the mechanical signal is only encoded on the phase quadrature. The second factor of two arises because the mechanical peak appears four times in the heterodyne power spectrum, while only twice in the homodyne power spectrum. Secondly, and more importantly, where homodyne detection yields a symmetrised mechanical power spectral density, the mechanical components in the heterodyne power spectral density are asymmetric between the positive and negative sides of the local oscillator detuning Δ_{LO} and match the quantum power spectral

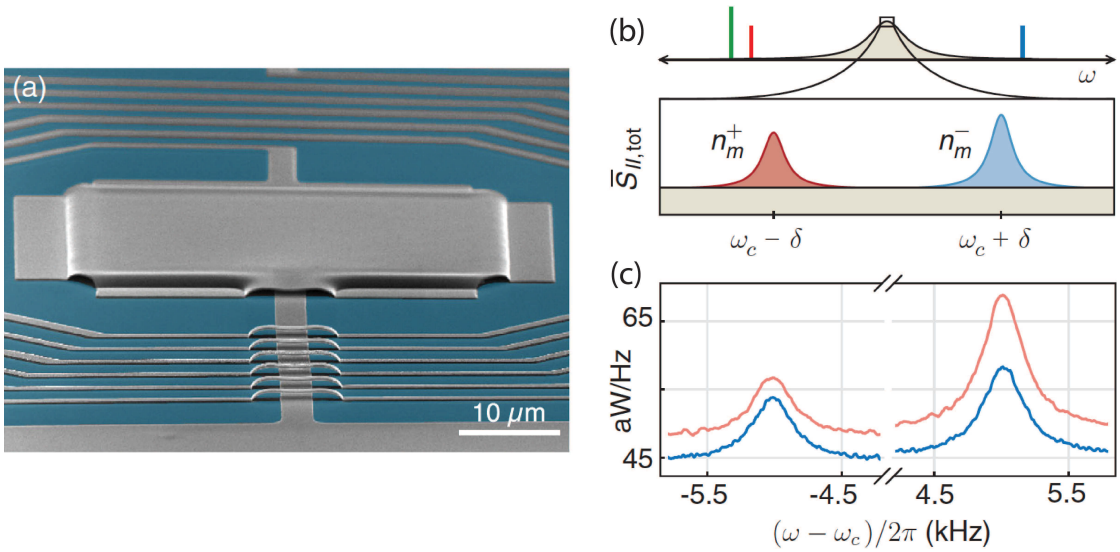

FIGURE 3.4 Sideband asymmetry experiment of [308]. (a) Bulk element superconducting microwave optomechanical device. (b) Illustration of heterodyne detection power spectrum. (c) Observed sideband asymmetry in the heterodyne power spectrum at $\bar{n}_b = 0.6$ (light grey) and $\bar{n}_b = 2.5$ (dark grey).

density of the mechanical oscillator itself. Heterodyne detection, therefore, allows the quantum asymmetry in the mechanical power spectrum to be directly probed.

Sideband asymmetry has been experimentally explored in a variety of cavity optomechanical systems, including, for example, phononic-photonic crystals [244], intracavity cold atom clouds [48], and superconducting microwave optomechanical systems [308]. Figure 3.4 shows the sideband asymmetry observed for a superconducting cavity optomechanical system cooled to millikelvin temperatures in a dilution refrigerator and further cooled using resolved sideband cooling (see Section 4.2.2) [308].

3.3.6.3 *Characterisation of optomechanical parameters*

Homodyne and heterodyne detection are valuable tools to characterise many of the important parameters in quantum optomechanical systems, the most important generally being the optomechanical cooperativity C and the mechanical occupancy $\bar{n}$. Appendix A discusses some useful methods to characterise these parameters that utilise the optical shot noise level and sideband asymmetry as a form of quantum ruler to achieve accurate calibration.

3.4 STANDARD QUANTUM LIMIT ON MECHANICAL POSITION MEASUREMENT

Now that we have determined the detected power spectral density of the output field of a cavity optomechanical system, including the radiation pressure induced measurement back-action on the mechanical oscillator, we are in a position to rigorously derive the standard quantum limit to optomechanical sensing which was first introduced for the case of a free mass in Section 3.1.

We being by renormalising the phase quadrature of the output field (Eq. (3.39)) into units of mechanical position:

$$\begin{aligned}\hat{Q}_{\rm det}(\omega) &\equiv \frac{\hat{X}^{\pi/2}_{\rm det}(\omega)}{2\sqrt{\Gamma C_{\rm eff}}} \\ &= \underbrace{\hat{Q}^{(0)}(\omega)}_{\text{mechanics}} - \underbrace{\frac{1}{2\sqrt{\Gamma C_{\rm eff}}}\left(\frac{\kappa/2+i\omega}{\kappa/2-i\omega}\right)\hat{Y}_{\rm in}(\omega)}_{\text{measurement noise}} - \underbrace{2\sqrt{\Gamma C_{\rm eff}}\chi(\omega)\hat{X}_{\rm in}(\omega)}_{\text{back-action noise}}.\end{aligned} \tag{3.50}$$

It is evident that, any estimate of the mechanical position from measurements on the output field will be contaminated by both the phase and amplitude quadratures of the input field. The phase quadrature contributes the usual measurement noise – or shot noise – familiar to many optical systems and sensors. The amplitude quadrature enters, in contrast, as a form of measurement back-action noise induced by the radiation pressure driving the mechanical motion (as we saw earlier in Section 3.2). Combined, these two noise sources are responsible for the standard quantum limit of measurement precision.

Again limiting ourselves to the case of coherent optical driving, where $S_{X_{\rm in}X_{\rm in}}(\omega) = S_{Y_{\rm in}Y_{\rm in}}(\omega) = 1/2$ and $\bar{S}_{X_{\rm in}Y_{\rm in}}(\omega) = 0$, the total homodyne detection noise power spectral density $\bar{S}_{\rm det}(\omega)$ due to measurement imprecision and back-action can be shown from Eq. (3.50) to be

$$\bar{S}_{\rm det}(\omega) = \frac{1}{8\eta\Gamma|C_{\rm eff}|} + 2\Gamma\left|\chi(\omega)\right|^2|C_{\rm eff}|\,, \tag{3.51}$$

where, similar to our earlier treatment of homodyne and heterodyne detection, we have introduced the parameter η to account for the total detection efficiency of the measurement including both escape efficiency from the optical cavity and losses afterwards. Recognising that the mechanical position operator $\hat{q} = \sqrt{2}x_{zp}\hat{Q}$, this noise floor can be expressed in terms of the absolute position of the oscillator via $\bar{S}_{q_{\rm det}q_{\rm det}}(\omega) = 2x_{zp}^2\bar{S}_{\rm det}(\omega)$, with the result having units of meters squared per hertz. Note also that, by limiting ourselves to both on-resonance optical driving ($\Delta = 0$), and the case where there are no correlations between the input quadratures of the bath, we are omitting important physics that provides a route to enhanced measurement precision. We consider these situations in detail in Section 5.4.

It is clear from Eq. (3.51) that, since the optical measurement noise decreases with increasing optomechanical cooperativity and the back-action

noise increases with increasing cooperativity, an optimum cooperativity exists that minimises the total noise in the displacement measurement. This optimum is achieved at

$$\left|C_{\rm eff}^{\rm opt}\right| = \frac{1}{4\eta^{1/2}\Gamma|\chi(\omega)|}. \tag{3.52}$$

At the interaction strength given in Eq. (3.52) the measurement and back-action noise terms are exactly balanced, with the total detection uncertainty given by

$$\bar{S}_{\rm det}^{\rm opt}(\omega) = \frac{|\chi(\omega)|}{\eta^{1/2}}. \tag{3.53}$$

We see that, even with the optimum choice of interaction strength, probing the mechanical oscillator necessarily introduces additional noise. Since the mechanical susceptibility $\chi(\omega)$ is largest on resonance, this noise is maximised on resonance (see Fig. 3.5). The detection noise decreases with increasing measurement efficiency, and as $\eta \to 1$ reaches the *standard quantum limit*

$$\bar{S}_{\rm det}^{\rm SQL}(\omega) = |\chi(\omega)|\,, \tag{3.54}$$

which quantifies the best measurement precision that can be achieved for a given mechanical susceptibility in the absence of quantum correlations or back-action evading measurements.[6]

It is worth noting that in the free-mass limit where $\omega \gg \{\Omega, \Gamma\}$ relevant for example to gravitational wave interferometers (see Section 3.5), when normalised into absolute position units by multiplying through by $2x_{zp}^2$ the standard quantum limit of Eq. (3.54) is independent of both the mechanical resonance frequency and decay rate; only depending on the mechanical oscillator via its mass m.

Exercise 3.7 *Show this result.*

3.4.1 Incident power required to reach the standard quantum limit

Practically, it is useful to know the level of incident optical power required to reach the standard quantum limit at the mechanical resonance frequency, which we define as $P^{\rm SQL}$. The optomechanical cooperativity which balances measurement and back-action noise can be re-expressed as an optimal intracavity optical coherent amplitude $\alpha^{\rm opt}$ using Eq. (3.13), with the result

$$|C_{\rm eff}^{\rm opt}(\Omega)| = \frac{1}{4\eta^{1/2}} = \frac{4{\alpha^{\rm opt}}^2 g_0^2}{\kappa\Gamma\left[1+(2\Omega/\kappa)^2\right]}. \tag{3.55}$$

[6] Note that it is important to distinguish the *optomechanical* standard quantum limit discussed here from a different *metrological* standard quantum limit discussed widely in the quantum metrology literature. The former results from a balance between optical shot noise and radiation pressure noise. The latter is the result only of optical shot noise and is valid in the usual regime of photon flux low enough not to introduce significant radiation pressure noise. A rough formulation of the latter is that it is the optimal sensitivity possible in a linear measurement using coherent light in the absence of radiation pressure noise.

Using Eq. (2.43) the intracavity amplitude α can itself be related to the optical power P in watts incident on an optical cavity via

$$P = \hbar\Omega_L \left|\alpha_{\rm in}\right|^2 \tag{3.56}$$

$$= \frac{\hbar\Omega_L\kappa}{4\eta_{\rm esc}}\left[1+\left(\frac{2\Delta}{\kappa}\right)^2\right]\alpha^2, \tag{3.57}$$

where the escape efficiency $\eta_{\rm esc} = \kappa_{\rm in}/\kappa$,[7] and as defined earlier, Ω_L is the laser frequency. Consequently, the incident optical power required to optimise the on-resonance ($\omega = \Omega$) measurement precision is

$$P^{\rm opt} = \frac{\hbar\Omega_L\Gamma\kappa^2}{64g_0^2\,\eta^{1/2}\eta_{\rm esc}}\left[1+\left(\frac{2\Delta}{\kappa}\right)^2\right]\left[1+\left(\frac{2\Omega}{\kappa}\right)^2\right], \tag{3.58}$$

where the terms in square brackets are corrections due to the cavity detuning and resolved-sideband suppression of the optomechanical interaction. The on-resonance standard quantum limit is reached when the detection is perfectly efficient ($\eta = \eta_{\rm esc} = 1$), with $P^{\rm SQL} \equiv P^{\rm opt}(\eta = \eta_{\rm esc} = 1)$. Taking parameters often found in cavity optomechanical systems of $\Omega_L/2\pi = 2\times10^{14}$ Hz, $\kappa/2\pi =$ 10 MHz, $\Delta = 0$, $\Omega/2\pi = 10$ MHz, $\Gamma/2\pi = 1$ kHz, and $g_0/2\pi = 100$ Hz, we find that in this particular case $P^{\rm SQL} \approx 700$ nW.

3.4.2 Dependence of detection noise spectrum on incident power

The detection noise power spectral density $\bar{S}_{\rm det}(\omega)$ is shown in Fig. 3.5 for a range of incident optical powers and perfect detection efficiency. It can be seen that for incident powers well below $P^{\rm SQL}$ the detection noise is spectrally flat. A Lorentzian peak appears near the mechanical resonance frequency as the incident power increases. When the incident power equals $P^{\rm SQL}$ the detection precision saturates the standard quantum limit on resonance but remains above it off resonance.

The back-action noise degrades the on-resonance detection precision once the incident power exceeds $P^{\rm SQL}$. However, the off-resonance precision continues to improve, and, in the limit of perfect detection efficiency ($\eta = 1$), can reach the standard quantum limit. The frequencies at which this occurs can be found by equating the detection noise power spectral density in Eq. (3.51) to the standard quantum limit of Eq. (3.54) and solving for ω, with the result

$$\frac{\omega}{\Omega} = \left[1 \pm \frac{1}{Q}\sqrt{\left(\frac{P}{P^{\rm SQL}}\right)^2 - 1}\right]^{1/2}. \tag{3.59}$$

Exercise 3.8 *Derive Eq. (3.59).*

[7] The total efficiency $\eta = \eta_{\rm esc}\eta_{\rm det}$ is the product of escape efficiency and the detection efficiency of photons that do escape from the cavity.

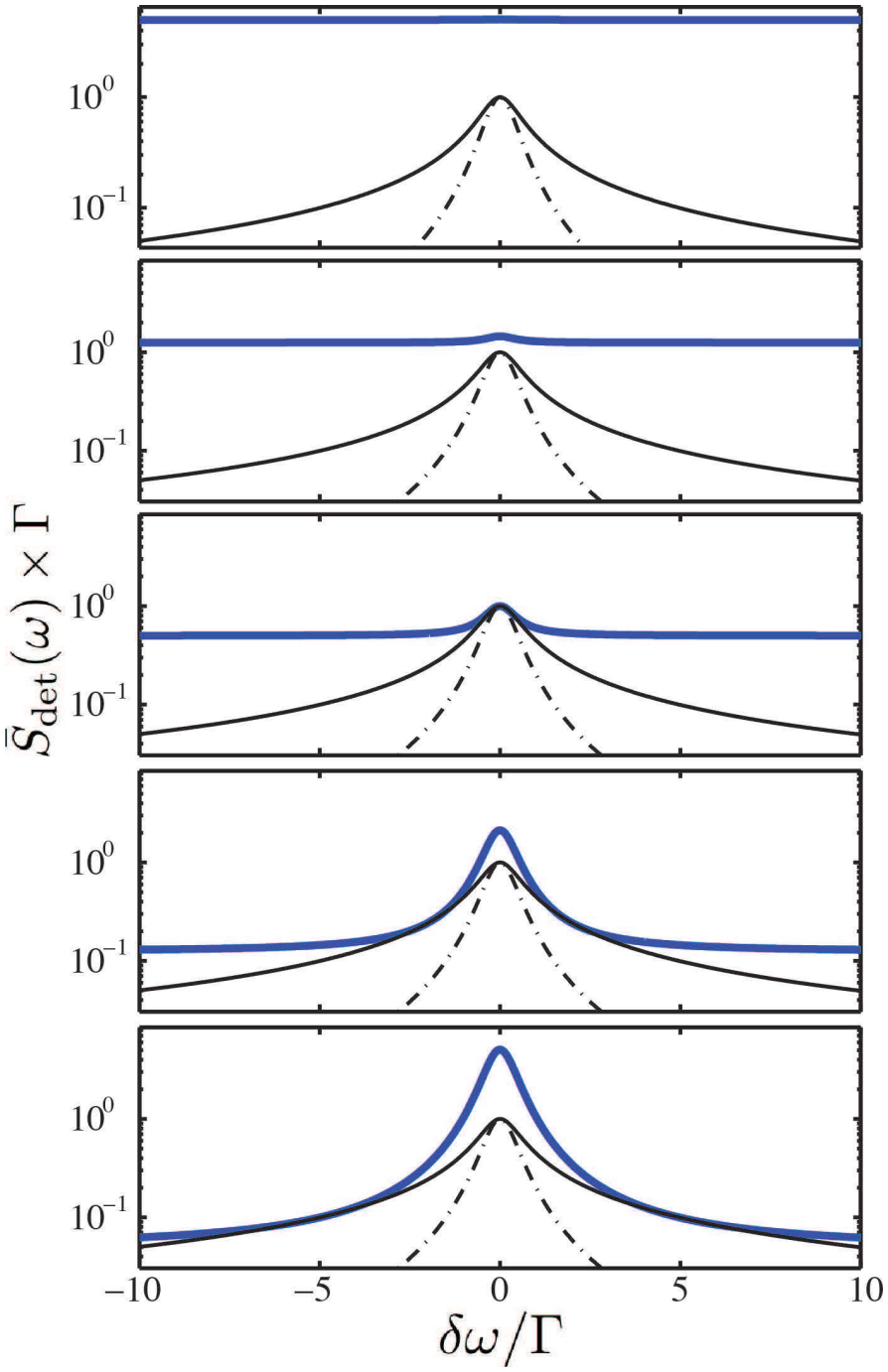

FIGURE 3.5 Total detection noise power spectral density $\bar{S}_{\rm det}(\omega)$ as a function of frequency, for various incident optical powers and perfect efficiency ($\eta = \eta_{\rm esc} = 1$). The frequency axis is centred on the mechanical resonance frequency with $\delta\omega = \omega - \Omega$. Thick solid curve: $\bar{S}_{\rm det}(\omega)$, thin solid curve: standard quantum limit $\bar{S}^{\rm SQL}_{\rm det}(\omega)$, thin dot-dashed curve: bath zero-point motion variance $\bar{S}^{\rm ZPL}_{\rm det}(\omega)$. For each trace the mechanical quality factor $Q = \Omega/\Gamma = 1000$, while from top to bottom $P/P^{\rm SQL} = \{0.1, 0.4, 1, 4, 10\}$.

The higher frequency solution is real as long as $P/P^{\mathrm{SQL}} \geq 1$, showing that once the incident power is sufficient to exceed the on-resonance standard quantum limit, in the limit of perfect efficiency there always exists a frequency above the mechanical resonance frequency at which the standard quantum limit is reached. If the additional criterion $Q^2 \geq (P/P^{\mathrm{SQL}})^2 - 1$ is satisfied, the standard quantum limit can also be reached at a second frequency beneath the mechanical resonance.

3.4.3 Optomechanical system as a probe of the mechanical bath

Notice that since the standard quantum limit of Eq. (3.54) is a function of the mechanical susceptibility, it is device dependent. That is to say, in a practical setting, if one wishes to enhance the precision of a measurement beyond the standard quantum limit of a particular device, this can be pursued not only by utilising quantum measurement techniques (as discussed in Chapter 5), but also by designing a device with smaller susceptibility at the frequencies of interest, or by altering the dynamics of the oscillator – for instance via dynamical optomechanical effects [43, 42, 155, 259, 296, 195, 197] – to directly modify the susceptibility. An alternative and more fundamental bound arises from thinking about optical measurements of the position of a mechanical oscillator as an indirect probe of the mechanical bath variable $\hat{P}_{\mathrm{in}}$. That is, the mechanical bath drives the mechanical oscillator and the optical field reads out the resulting motion. It is then natural to compare the precision of such a measurement to the zero-point uncertainty of the bath

$$\bar{S}^{(\bar{n}=0)}_{P_{\mathrm{in}}P_{\mathrm{in}}}(\omega) = \frac{\omega}{2\Omega}, \tag{3.60}$$

where here to retain validity well away from the mechanical resonance frequency we have chosen not make the usual quantum optics approximation, instead taking the zero temperature limit of the general bath power spectral densities in Eqs. (1.98).

When driven by the zero temperature bath of Eq. (3.60), the mechanical oscillator power spectral density in the absence of radiation pressure can be found from Eq. (3.41) to be

$$\bar{S}^{(\bar{n}=0)}_{QQ}(\omega) = \bar{S}^{\mathrm{ZPL}}_{\mathrm{det}}(\omega) = \frac{\omega}{Q}|\chi(\omega)|^2, \tag{3.61}$$

where, as usual, $Q = \Omega/\Gamma$ is the mechanical quality factor. We will see in Chapter 5 that this zero-point mechanical power spectral density presents a limit to the precision of continuous quantum measurements of a mechanical oscillator, even in the presence of quantum correlations. We term it the *zero-point limit*. A measurement that saturates this limit is just sufficient to resolve the zero-point uncertainty of the mechanical bath.

Comparing the zero-point limit to the standard quantum limit of

Eq. (3.54), we find that

$$\bar{S}^{\mathrm{ZPL}}_{\mathrm{det}}(\omega)\Big/\bar{S}^{\mathrm{SQL}}_{\mathrm{det}}(\omega) = \frac{\omega}{Q}|\chi(\omega)|. \tag{3.62}$$

The two limits are equal at the mechanical resonance frequency where the mechanical susceptibility is at its maximum ($\chi(\Omega) = 1/\Gamma$), but diverge off-resonance where measurements at the standard quantum limit are incapable of resolving the mechanical zero-point fluctuations (see Fig. 3.5). As we will see in Chapter 5, quantum correlations in principle allow the zero-point limit to be reached at all frequencies; while back-action evading techniques allow it to be surpassed.

3.4.4 Standard quantum limit for displacement measurement

In many scenarios one is interested in measuring a classical signal encoded on the motion of a mechanical oscillator via, for example, an external force. In this case, the environmentally driven motion of the mechanical oscillator presents an additional source of noise. The symmetrised power spectral density of the detected mechanical position $\hat{Q}_{\mathrm{det}}$ from Eq. (3.50) then determines the total noise floor of the measurement. This is given by

$$\begin{aligned}\bar{S}_{Q_{\mathrm{det}}Q_{\mathrm{det}}}(\omega) &= \bar{S}^{(0)}_{QQ}(\omega) + \bar{S}_{\mathrm{det}}(\omega) &(3.63)\\ &= \frac{\omega}{Q}|\chi(\omega)|^2(2\bar{n}(\omega)+1) + \bar{S}_{\mathrm{det}}(\omega), &(3.64)\end{aligned}$$

where we have again used the general bath power spectral densities in Eqs. (1.98), and the general frequency dependent bath occupation $\bar{n}(\omega)$ is defined in Eq. (1.85). Three interesting regimes are evident from inspection of this expression, in conjunction with Eq. (3.51) for $\bar{S}_{\mathrm{det}}(\omega)$. At optical powers low enough that $|C_{\mathrm{eff}}| < 8\eta\Gamma|\chi(\omega)|^2(2\bar{n}(\omega)+1)\,\omega/Q$, the precision of the measurement is insufficient to resolve even the thermal motion of the mechanical oscillator, and measurement noise dominates; when $8\eta\Gamma|\chi(\omega)|^2(2\bar{n}(\omega)+1)\,\omega/Q < |C_{\mathrm{eff}}| < (\bar{n}(\omega)+1/2)\,\omega/\Omega$, mechanical thermal noise dominates; and when $|C_{\mathrm{eff}}| > (\bar{n}(\omega)+1/2)\,\omega/\Omega$, back-action noise dominates.

Figure 3.6 shows the detected mechanical power spectral density $\bar{S}_{Q_{\mathrm{det}}Q_{\mathrm{det}}}(\omega)$ at the mechanical resonance frequency calculated from Eq. (3.64) as a function of incident optical power, phonon occupancy, and optical efficiency. As can be seen from Fig. 3.6a, with perfect efficiency the power spectral density is minimised at an incident power matching the on-resonance P^{SQL}. At lower powers optical measurement noise dominates, and at higher power back-action noise dominates, with a plateau present around P^{SQL} due to the thermal occupancy of the mechanical oscillator. Fig. 3.6b shows that the effect of measurement inefficiency is to increase the optical measurement noise, increasing the minimum achievable power spectral density, and pushing it to incident powers above P^{SQL}.

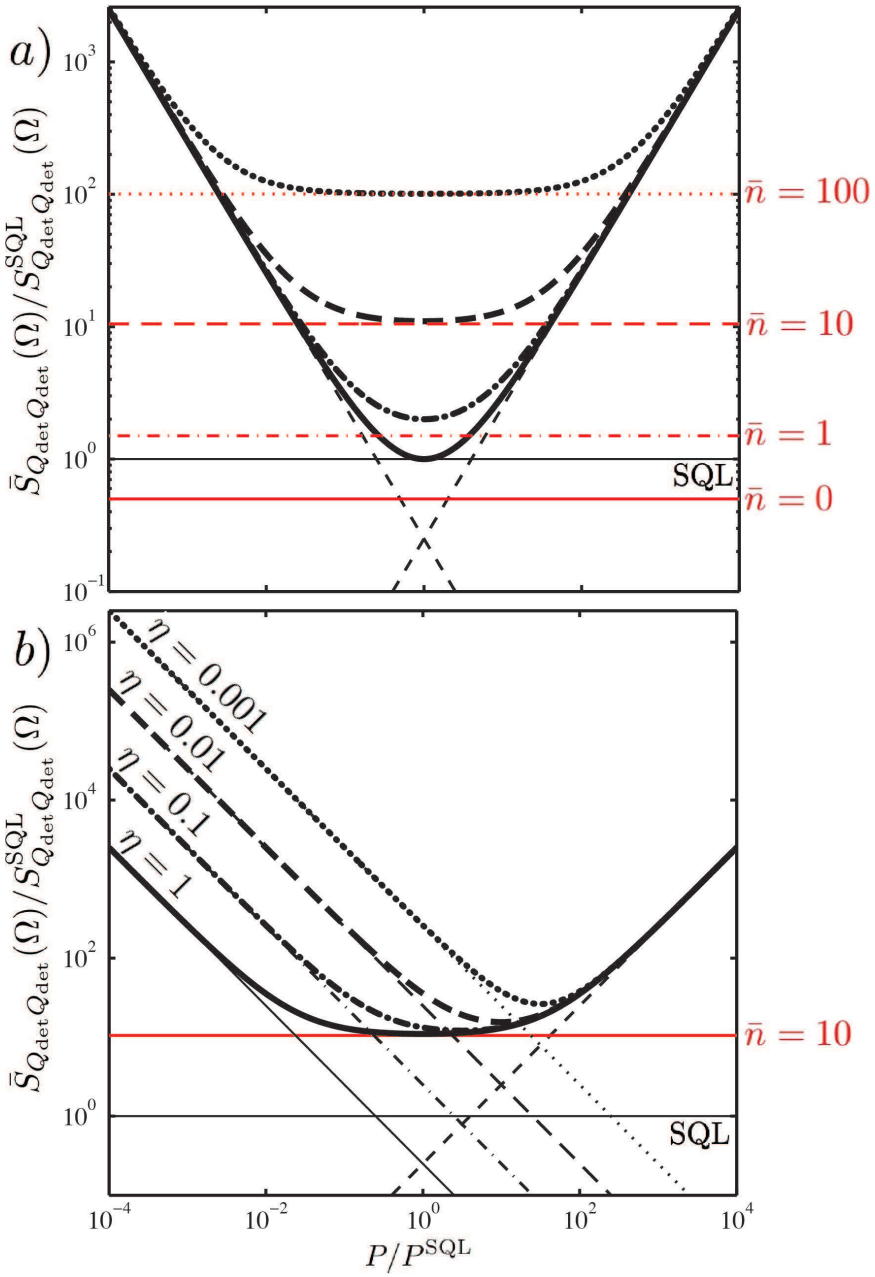

FIGURE 3.6 On-resonance power spectral density of continuous position measurement on a mechanical oscillator as a function of incident optical power, showing the standard quantum limit. (a) Power spectral density with varying thermal occupancy and $\eta = 1$, showing that the standard quantum limit (SQL) is reached when the mechanical oscillator is in its ground state and incident optical power equals $P^{\rm SQL}$. (b) Power spectral density with varying optical measurement efficiency η and fixed on-resonance thermal occupancy $\bar{n}(\Omega) = 10$, showing that, as the efficiency is decreased, the optical power that attains the minimum power spectral density is increased and the overall measurement sensitivity is degraded. Dashed black lines with negative slope: measurement noise. Dashed black lines with positive slope: back-action noise.

In the limit that the thermal noise from the mechanical oscillator is negligible ($\bar{n} \ll 1$) and the optical measurement is performed with perfect efficiency ($\eta = 1$), the optimal measurement precision reaches the standard quantum limit for displacement measurement

$$\bar{S}^{\mathrm{SQL}}_{Q_{\mathrm{det}}Q_{\mathrm{det}}}(\omega) = \frac{\omega}{Q}|\chi(\omega)|^2 + |\chi(\omega)|\,, \tag{3.65}$$

at the optimal effective cooperativity of Eq. (3.52). At the mechanical resonance frequency the susceptibility $|\chi(\Omega)| = 1/\Gamma$. Remembering that the quality factor $Q \equiv \Omega/\Gamma$, we therefore see that a minimum consequence of continuous quantum measurement of the position of a mechanical oscillator is to introduce additional noise at the mechanical frequency with magnitude equal to the on-resonance mechanical zero-point fluctuations of the oscillator – i.e. to double the imprecision above that dictated by zero-point motion. As was illustrated in the simple example of a free mass in Section 3.1, this additional noise is required by quantum mechanics to ensure that the measurement does not violate the uncertainty principle.

Any realistic optomechanical system will have some mechanical thermal noise and optical inefficiencies, and therefore – without back-action evading measurements or non-classical correlations – will not achieve the standard quantum limit. Choosing the optimal effective cooperativity of Eq. (3.52), the optimal precision of a continuous displacement measurement in the presence of such imperfections can be found from Eq. (3.64) to be

$$\bar{S}^{\mathrm{opt}}_{Q_{\mathrm{det}}Q_{\mathrm{det}}}(\omega) = \bar{S}^{\mathrm{SQL}}_{Q_{\mathrm{det}}Q_{\mathrm{det}}}(\omega) + \bar{S}^{\mathrm{excess}}_{Q_{\mathrm{det}}Q_{\mathrm{det}}}(\omega), \tag{3.66}$$

where the excess noise above the standard quantum limit is

$$\bar{S}^{\mathrm{excess}}_{Q_{\mathrm{det}}Q_{\mathrm{det}}}(\omega) = \frac{2\bar{n}(\omega)\,\omega}{Q}|\chi(\omega)|^2 + |\chi(\omega)|\left(\eta^{-1/2} - 1\right). \tag{3.67}$$

It is natural to ask whether there are realistic situations in which the effects of thermal noise and inefficiencies are negligible, or in other words when is the criterion $\bar{S}^{\mathrm{excess}}_{Q_{\mathrm{det}}Q_{\mathrm{det}}}(\omega) \ll \bar{S}^{\mathrm{SQL}}_{Q_{\mathrm{det}}Q_{\mathrm{det}}}(\omega)$ satisfied? There are two particularly interesting regimes in which to analytically examine this question. The first is the on-resonance regime ($\omega = \Omega$), where the criterion becomes that

$$\bar{n} + \frac{\eta^{-1/2} - 1}{2} \ll 1. \tag{3.68}$$

Therefore, the on-resonance standard quantum limit of displacement measurement can only be approached if both the mechanical bath is near its ground state, with thermal occupancy $\bar{n} \equiv \bar{n}(\Omega) \ll 1$, and the efficiency $\eta^{-1/2} - 1 \ll 2$. The efficiency requirement is not especially stringent, with the left- and right-hand sides of the inequality equal when $\eta = 1/9$. However, the requirement that the mechanical bath be close to its ground state precludes reaching the standard quantum limit in many scenarios.

The second interesting regime is the *free-mass regime*, where the frequencies of interest lie far above the mechanical resonance frequency, i.e., $\omega \gg \{\Omega, \Gamma\}$. In this regime, the mechanical susceptibility can be approximated as $|\chi(\omega)| = \Omega/\omega^2$, and both thermal noise and inefficiencies are negligible if

$$2\bar{n}(\omega)\frac{\Gamma}{\omega} + \eta^{-1/2} - 1 \ll 1. \tag{3.69}$$

That is, the two requirements $\bar{n}(\omega) \ll \omega/2\Gamma$ and $\eta^{-1/2} - 1 \ll 1$ must be satisfied. Quite strikingly, while, in the on-resonance case, cooling to near the ground state is necessary to approach the standard quantum limit, we see here that the thermal occupancy is always negligible sufficiently far into the free-mass regime. Therefore, it is possible for the standard quantum limit to impose the dominate constraint on precision even for a hot mechanical oscillator. The reason is that, as can be seen from inspection of Eqs. (3.67) and (3.54), the thermal noise decreases faster with frequency ω than the detection noise. The (much less significant) factor of two difference in the efficiency criterion compared to the on-resonance case arises similarly, because the mechanical zero-point motion decreases faster than the detection noise as ω increases (see Eq. (3.65)). Consequently, while the contributions to the standard quantum limit from zero-point motion and detection noise are exactly equal on-resonance, the zero-point motion contribution becomes negligible sufficiently far into the free-mass regime.

We can gain more intuition about the thermal occupancy requirement in the free-mass regime by making the high temperature approximation $\bar{n}(\omega) \approx k_B T/\hbar\omega$, in which case the condition becomes

$$\frac{\omega^2}{\Gamma} > \frac{2k_B T}{\hbar}. \tag{3.70}$$

This bears a close resemblance to the condition for quantum coherent oscillation of a mechanical oscillator given in Eq. (2.25). Here, however, the significance of the condition is that, for quantum noise to dominate, less than half a quanta of thermal heating must be introduced within one period of oscillation at frequency ω.

The detected mechanical oscillator position power spectral density is compared to the standard quantum limit of displacement measurement as a function of frequency in Fig. 3.7 (*left column*). The top subplot shows the power spectrum for incident power well below the standard quantum limit. In this regime the contribution from mechanical thermal motion may be resolvable above the measurement noise (as is the case here), but the contribution from mechanical zero-point fluctuations is not. The second subplot shows the power spectrum when the incident power $P = P^{\mathrm{SQL}}$. Here, the mechanical zero-point fluctuations are resolvable above the measurement noise, but remain obscured, in this case, by mechanical thermal fluctuations. As the incident power increases further, the contributions to the power spectrum from mechanical thermal and vacuum fluctuations are reduced relative to the optical

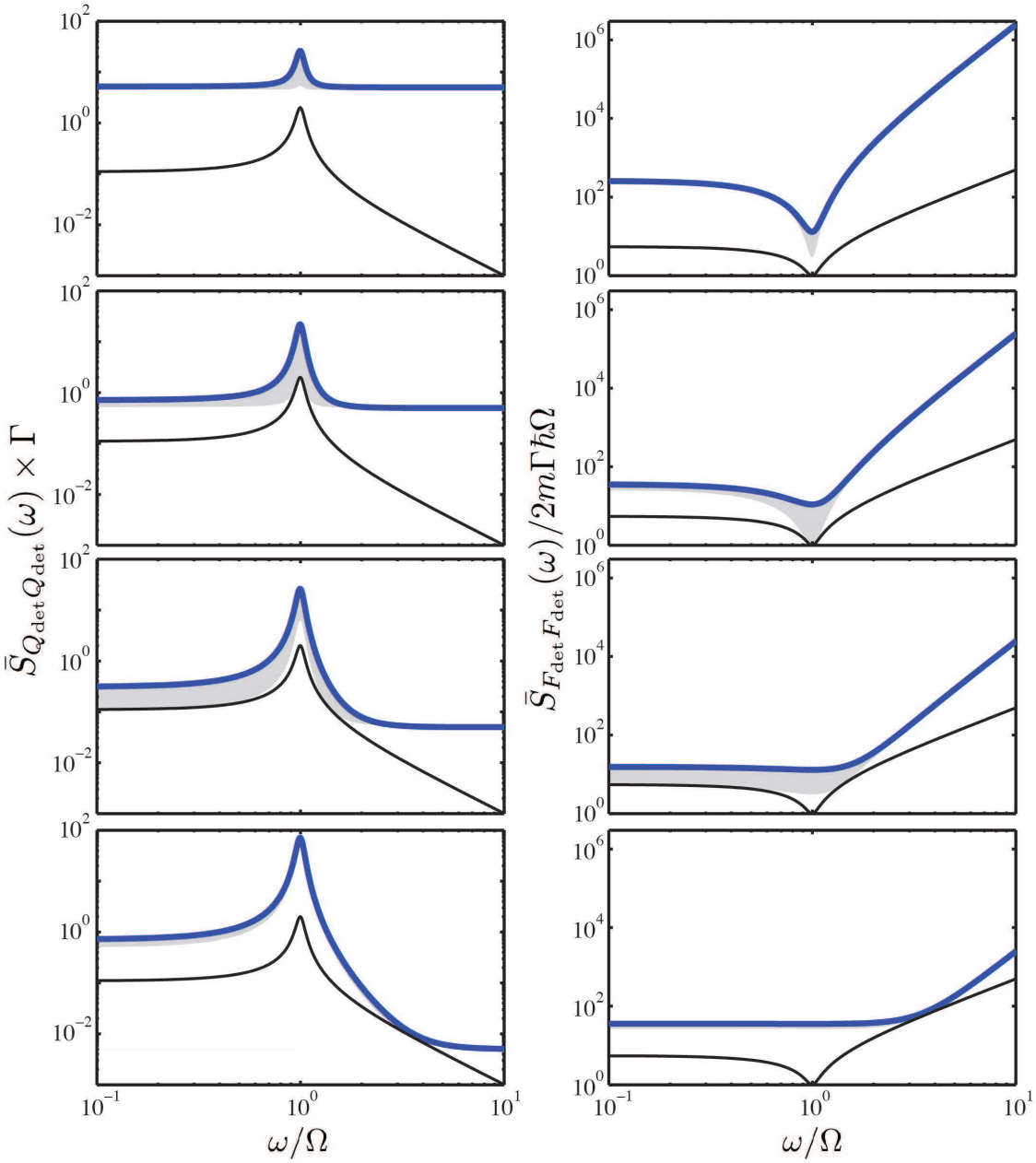

FIGURE 3.7 Detected mechanical position (left column) and force (right column) power spectral densities as a function of frequency. Bold line: power spectral density. Thin line: standard quantum limit. Shaded region: thermal contribution to power spectral density. From top to bottom, the vertically arrayed subplots have increasing incident powers of $P/P^{\rm SQL} = \{0.1, 1, 10, 100\}$. The mechanical oscillator thermal occupancy and quality factor are, respectively, $Q = 10$ and $\bar{n}(\Omega) = 10$, and the optical measurement efficiency is $\eta = 1$.

back-action contribution. It can be seen that – as expected given the $\bar{n} = 10$ thermal occupancy of the oscillator – the detected mechanical power spectral density never reaches the standard quantum limit at the mechanical resonance frequency. However, as we have observed earlier in this section, thermal occupancy does not preclude approaching the standard quantum limit away from the mechanical resonance. Indeed, this is possible, as shown in the bottom subplot.

3.5 STANDARD QUANTUM LIMIT FOR GRAVITATIONAL WAVE INTERFEROMETRY

Most relevant optomechanical measurements involve the optical transduction of a force applied to the mechanical oscillator, as will be discussed in Section 3.6. However, in some circumstances it is desired to measure direct modulations of the cavity path length rather than modulations that result from a force on the oscillator. The most notable example is gravitational wave interferometry, where an itinerant gravitational wave modulates the relative arm lengths of the interferometer directly. Here, for consistency, we will derive the standard quantum limit for path length measurement using an optical cavity. While gravitational wave detectors are interferometers, the essential effect is the same, and within a scaling factor accounting for the different geometry the results are identical. In an optical cavity, the net effect of a path length change is to alter the resonance frequency of the cavity, pushing it off resonance with the incident laser light. To model the standard quantum limit, we must therefore introduce an additional detuning term Δ_{sig} into the Hamiltonian. To do this, we begin with the nonlinearised Hamiltonian of Eq. (2.18), substituting in the total detuning $\Delta \to \Delta + \Delta_{\mathrm{sig}}$. The additional cavity detuning term is then $\hbar\Delta_{\mathrm{sig}} a^\dagger a$. We linearise this term in the usual way by making the substitution $a \to \alpha + a$, where α is the steady-state expectation value of the original operator, and neglecting the operator product term to find

$$\hbar\Delta_{\mathrm{sig}} a^\dagger a = \hbar\Delta_{\mathrm{sig}} \left(\alpha^2 + \sqrt{2}\alpha\hat{X}\right). \tag{3.71}$$

The first term in this expression is a constant in the steady-state and therefore has no effect on the steady-state dynamics and can be safely neglected. Setting the cavity detuning to zero when no signal is present, the linearised optomechanical Hamiltonian of Eq. (2.41) then becomes

$$\hat{H} = \frac{\hbar\Omega}{2}\left(\hat{Q}^2 + \hat{P}^2\right) + \sqrt{2}\hbar\alpha\Delta_{\mathrm{sig}}\hat{X} + 2\hbar g\hat{X}\hat{Q}. \tag{3.72}$$

Through geometric arguments the cavity detuning can be related to the change in path length l and strain h via

$$\frac{\Delta_{\mathrm{sig}}}{\Omega_c} = -\frac{l}{L} = -h, \tag{3.73}$$

where L and Ω_c are the cavity path length and resonance frequency, respectively. We then get

$$\hat{H} = \frac{\hbar\Omega}{2}\left(\hat{Q}^2 + \hat{P}^2\right) - \sqrt{2}\hbar\Omega_c\alpha h\hat{X} + 2\hbar g\hat{X}\hat{Q}. \tag{3.74}$$

The Langevin equations of motion derived from this Hamiltonian are the same as those from Eq. (2.41) except that an additional coherent displacement proportional to the strain h is introduced into Eq. (3.9b), which becomes

$$\dot{\hat{Y}} = -\frac{\kappa}{2}\hat{Y} + \sqrt{2\kappa}\hat{Y}_{\rm in} + \sqrt{2}\Omega_c\alpha h - 2g\hat{Q}. \tag{3.75}$$

We can see immediately from this expression that the effect of the strain is identical to that of the position of the mechanical oscillator $\hat{Q}$ except scaled by a factor $-\Omega_c/\sqrt{2}g_0$ (remember that $g \equiv \alpha g_0$). Consequently, the strain sensitivity of a cavity optomechanical system can be related to sensitivity to displacements of the mechanical oscillator via

$$\bar{S}_{hh}(\omega) = 2\left(\frac{g_0}{\Omega_c}\right)^2 \bar{S}_{Q_{\rm det}Q_{\rm det}}(\omega). \tag{3.76}$$

This expression can be simplified to some degree in the special case of a Fabry–Pérot cavity. We showed in Section 2.3 that, for a Fabry–Pérot cavity, $g_0 = x_{zp}\Omega_c/L$. Defining the zero-point strain $h_{zp} \equiv x_{zp}/L$, we then have

$$\bar{S}_{hh}(\omega) = 2h_{zp}^2\bar{S}_{Q_{\rm det}Q_{\rm det}}(\omega). \tag{3.77}$$

Gravitational wave interferometers operate in the free-mass regime where $\omega \gg \{\Omega, \Gamma\}$, with their mirrors mounted on large low frequency suspension systems. In this limit the susceptibility $|\chi(\omega)| \approx \Omega/\omega^2$. Substituting this into Eq. (3.65) for the position standard quantum limit and using the relation in Eq. (3.77), we then arrive at the standard quantum limit of strain sensing

$$\bar{S}_{hh}^{\rm SQL}(\omega) = \frac{2\Omega}{\omega^2}h_{zp}^2 \tag{3.78}$$

$$= \frac{\hbar}{mL^2\omega^2} \tag{3.79}$$

A similar result holds for strain sensing in a Michelson interferometer configuration, differing only by a factor of four [157]. We see that this limit scales favourably with the measurement frequency ω, the mass of the oscillator, and the cavity path length, while being independent of both the mechanical oscillator resonance frequency and mass. This motivates the use of long base-line interferometers with large mass end-mirrors in gravitational wave interferometry. For a cavity that has $L = 4$ km length, with one suspended mirror of mass $m = 1$ kg and a signal at $\omega/2\pi = 1$ kHz, Eq. (3.79) gives an impressive strain sensitivity of $\bar{S}_{hh}^{\rm SQL}(\omega)^{1/2}/2\pi = 10^{-24}$ Hz$^{-1/2}$. As discussed in the previous section, the suppression of thermal noise with increasing ω above the mechanical resonance frequency makes it feasible to reach such sensitivities in future gravitational wave interferometers.

3.6 STANDARD QUANTUM LIMIT FOR FORCE MEASUREMENT

While displacement measurements such as those discussed in the previous section have the significant advantage of exhibiting a suppression of thermal noise off resonance, in typical applications of mechanical oscillators it is the forces applied to the mechanical oscillator, rather than the displacements they induce, that are of primary interest. Uncertainties in displacement measurement can be straightforwardly recast in terms of external forces using Eqs. (1.94) and (3.17). Equation (1.94) allows us to relate the power spectral density of the external force driving the oscillator to the power spectral density of the dimensionless bath momentum operator as $\bar{S}_{FF}(\omega) = 2\Gamma m\hbar\Omega \bar{S}_{P_{\rm in}P_{\rm in}}(\omega)$, while from Eq. (3.17) we have $\bar{S}^{(0)}_{QQ}(\omega) = 2\Gamma|\chi(\omega)|^2 \bar{S}_{P_{\rm in}P_{\rm in}}(\omega)$. Consequently,

$$\bar{S}_{FF}(\omega) = \frac{\hbar m\Omega}{|\chi(\omega)|^2}\bar{S}^{(0)}_{QQ}(\omega). \tag{3.80}$$

Apart from establishing the coefficient converting a position power spectral density to a force power spectral density, this expression also makes clear that the precision of force measurements is, unsurprisingly, enhanced on resonance where the susceptibility $\chi(\omega)$ is at its maximum. Since the displacement and force power spectral densities are linearly related, Eq. (3.65) defines a standard quantum limit not only for displacement sensing, but also for force sensing. Cavity optomechanics experiments using the collective motion of a cold atom cloud cooled close to its ground state have recently demonstrated force sensing with precision within a factor of four of this limit [253].

Renormalising the displacement noise floor of Eq. (3.64) into newtons per root hertz by multiplying through by the coefficient $\hbar m\Omega/|\chi(\omega)|^2$ established in Eq. (3.80) yields the force noise floor of a cavity optomechanical force sensor

$$\bar{S}_{F_{\rm det}F_{\rm det}}(\omega) = 2m\Gamma\hbar\Omega\left[\frac{\omega}{\Omega}\left(\bar{n}(\omega)+\frac{1}{2}\right)+\frac{1}{16\eta\Gamma^2|\chi(\omega)|^2|C_{\rm eff}|}+|C_{\rm eff}|\right], \tag{3.81}$$

which is minimised for the same optimal effective cooperativity as given for displacement sensing in Eq. (3.52). The force power spectral density is shown as a function of frequency in the right-hand column of Fig. 3.7 for a range of cooperativity values, clearly displaying a minimum near the mechanical resonance frequency Ω and degrading away from resonance. This is in distinct contrast to the power spectral density of position sensing (Fig. 3.7 *left column*), which showed the reverse behaviour.

3.6.1 Bandwidth of optomechanical force sensing

The previous few sections show that measurement back-action introduces a fundamental quantum limit on the precision of mechanical oscillator based sensing. One might, therefore, think that there is no advantage to increasing

the effective cooperativity above the optimum given in Eq. (3.52). In Chapter 5 we will see that, for special forms of measurement such as *back-action evading measurements*, the back-action penalty can, as the name suggests, be evaded. A second – and perhaps even more significant – advantage of increasing interaction strength is improved measurement bandwidth. Figure 3.7 (*right column*) shows that, where for low cooperativity the mechanical force power spectral density is sharply peaked around Ω, as the cooperativity is raised, the power spectral density broadens and eventually becomes constant at frequencies below Ω, increasing the sensing bandwidth.

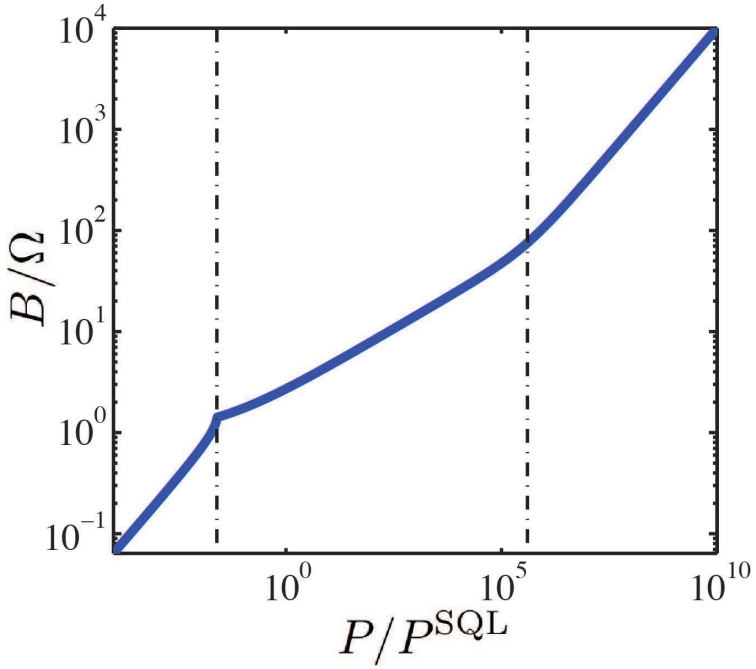

FIGURE 3.8 Bandwidth of cavity optomechanical force sensing as a function of incident power P in the limit where $\kappa \gg \omega$. Left-most vertical line: incident power at which the optical measurement noise is equal to the thermal noise at $\omega = 0$. Right-most vertical line: incident power at which back-action noise dominates thermal noise. The mechanical oscillator is taken to have a quality factor $Q = 100$ and thermal occupancy $\bar{n} = 10^5$, and the efficiency of the optical measurement is taken to be $\eta = 1$.

The force sensing bandwidth can reasonably be defined as the width of the region of frequency space over which the force noise power spectral density is within a factor of two of the minimum at $\omega = \Omega$. The frequencies $\omega^{\pm}_{3\,\mathrm{dB}}$ at which the force noise power spectral density is exactly a factor of two above the minimum can be determined analytically from Eq. (3.81) in the regime where they lie well within the cavity linewidth ($\omega \ll \kappa$), so that $C_{\mathrm{eff}}(\omega) \approx C$.

Making the quantum optics approximation that $(\bar{n}(\omega)+1/2)\omega/\Omega = \bar{n}(\Omega)+1/2$ they are found in this regime to be

$$\left(\frac{\omega^{\pm}_{3\,\mathrm{dB}}}{\Omega}\right)^2 = 1 - \frac{1}{2Q^2} \pm \frac{1}{Q}\left[\frac{1}{4Q^2} + 1 + 16\eta C\left(\bar{n} + \frac{1}{2} + C\right)\right]^{1/2}, \quad (3.82)$$

where, as always when the argument is omitted, $\bar{n} \equiv \bar{n}(\Omega)$.

Exercise 3.9 *Show this result.*

Clearly, as the cooperativity increases, the separation between the low, and high, frequency solutions becomes larger, and therefore the bandwidth increases. The higher-frequency solution is always real. The lower-frequency solution, on the other hand, becomes imaginary once the cooperativity is sufficiently high that the contributions to the power spectral density from mechanical thermal noise and optical noise become comparable at zero frequency. This transition occurs at a cooperativity of $C = Q^2[8\eta(2\bar{n}+1)]^{-1}$, at which point the sensing bandwidth extends all the way to $\omega = 0$.

Given the behaviour of the lower-frequency solution, the force sensing bandwidth B can be determined from Eq. (3.82) as

$$B = \omega^{+}_{3\,\mathrm{dB}} - \mathrm{real}\left\{\omega^{-}_{3\,\mathrm{dB}}\right\}. \quad (3.83)$$

This bandwidth has several different regimes of behaviour as the cooperativity increases, as illustrated in Fig. 3.8. At relatively low cooperativity, where $[16\eta(\bar{n}+1/2)]^{-1} \ll C \ll \{\bar{n}+1/2, Q^2[16\eta(\bar{n}+1/2)]^{-1}\}$ and the mechanical thermal noise is unresolved beneath the optical noise at zero frequency, the bandwidth can be shown to be

$$B = 4\Gamma\left[\eta C\left(\bar{n} + \frac{1}{2}\right)\right]^{1/2}, \quad (3.84)$$

scaling as $C^{1/2}$. Once the mechanical thermal noise is resolved, in the limit $Q^2/[16\eta C(\bar{n}+1/2)] \ll C \ll \bar{n}+1/2$, the bandwidth becomes

$$B = 2\sqrt{\Gamma\Omega}\left[\eta C\left(\bar{n} + \frac{1}{2}\right)\right]^{1/4}, \quad (3.85)$$

scaling as $C^{1/4}$; and when the measurement back-action dominates, in the limit $C \gg \{\bar{n}+1/2, Q/4\eta^{1/2}\}$, it is

$$B = 2\sqrt{\Gamma\Omega C}\,\eta^{1/4}, \quad (3.86)$$

scaling again as $C^{1/2}$. The reason for this improved bandwidth scaling in the back-action dominated regime is that, in additional to measurement noise that decreases as C^{-1} and allows the mechanical thermal noise to be resolved further from resonance, the back-action heating of the oscillator increases the

total mechanical noise relative to the optical measurement noise. This second effect increases the bandwidth by *decreasing* the sensitivity on resonance, rather than increasing it in the wings of the resonance. Never-the-less, it can be seen that, while the scaling changes with cooperativity, the general trend of increasing bandwidth with C remains, even in the regime where the measurement is dominated by measurement back-action.

3.6.2 Sensitivity of classical force sensing

Micro- and nano-mechanical oscillators are commonly used as force and inertial sensors. Such sensors typically operate in a regime where the mechanical thermal noise dominates on resonance, and where the quantum back-action noise on the sensor is negligible. In this case, taking the relevant high temperature limit where $\bar{n}(\omega) + 1/2 \approx k_B T/\hbar\omega$ we obtain an optical shot-noise limited force noise floor of

$$S^{\text{class}}_{F_{\text{det}}F_{\text{det}}}(\omega) = 2m\Gamma k_B T + \frac{m\hbar Q}{8\eta|\chi(\omega)|^2|C_{\text{eff}}|}. \tag{3.87}$$

The spectrally flat term on the left is the usual thermomechanical force sensing limit for micromechanical force sensors.[8] It can only be surpassed by engineering the bath coupled to the mechanical oscillator, for example, by cooling or squeezing it. The term on the right is the measurement noise floor, which has a minimum near the mechanical resonance frequency Ω and decreases as the optomechanical cooperativity increases. While the measurement noise appears to increase linearly with the mechanical quality factor Q, the mechanical susceptibility $\chi(\omega)$ is also a function of Q. In the limit that $\omega \gg \{\Omega, \Gamma\}$, for instance, $|\chi(\omega)|^2$ scales as Q^2 so that the measurement noise floor decreases as Q^{-1}. Substantial efforts have been made over many years in the nano- and micro-electromechanics community to both improve the measurement precision and thereby reach the thermomechanical noise dominated regime, and to reduce the noise floor in this regime by decreasing Γ and m [101].

One might think that the improved measurement precision provided, for example, by an optical cavity would provide no advantage in force sensing once the thermomechanical noise dominates the measurement. It is correct that improved measurement precision will not improve the force sensitivity at the peak of the mechanical resonance in this limit. However, as discussed in the previous section, improved precision will increase the frequency band over which the thermomechanical noise dominates measurement noise. This increases the bandwidth over which the maximum sensitivity can be achieved, and also allows improved sensitivity in measurements of broadband signals such as incoherent forces. This has allowed the demonstration of a

[8] Note that typically in the force sensing literature the decay rate is defined as the full-width-half-maximum of the mechanical resonance, and this results in a value equal to half the value used here. As a result, this classical force sensing limit is usually quoted as $S^{\text{class}}_{FF}(\omega) = 4m\Gamma k_B T$.

range of high bandwidth, high sensitivity, cavity optomechanical sensors, including force sensors [115, 213, 136], inertial sensors [164], and magnetometers [107, 106].